2014

AXIAL COMPRESSOR FLOW BEHAVIOR NEAR THE AERODYNAMIC STABILITY LIMIT

Bradley D. Butler

University of Kentucky, bdbutl3@g.uky.edu

Click here to let us know how access to this document benefits you.

STUDENT AGREEMENT:

I represent that my thesis or dissertation and abstract are my original work. Proper attribution has been given to all outside sources. I understand that I am solely responsible for obtaining any needed copyright permissions. I have obtained needed written permission statement(s) from the owner(s) of each third-party copyrighted matter to be included in my work, allowing electronic distribution (if such use is not permitted by the fair use doctrine) which will be submitted to UKnowledge as Additional File.

I hereby grant to The University of Kentucky and its agents the irrevocable, non-exclusive, and royalty-free license to archive and make accessible my work in whole or in part in all forms of media, now or hereafter known. I agree that the document mentioned above may be made available immediately for worldwide access unless an embargo applies.

I retain all other ownership rights to the copyright of my work. I also retain the right to use in future works (such as articles or books) all or part of my work. I understand that I am free to register the copyright to my work.

REVIEW, APPROVAL AND ACCEPTANCE

The document mentioned above has been reviewed and accepted by the student's advisor, on behalf of the advisory committee, and by the Director of Graduate Studies (DGS), on behalf of the program; we verify that this is the final, approved version of the student's thesis including all changes required by the advisory committee. The undersigned agree to abide by the statements above.

Bradley D. Butler, Student

Dr. Vincent R. Capece, Major Professor

Dr. James M. McDonough, Director of Graduate Studies

AXIAL COMPRESSOR FLOW BEHAVIOR NEAR
THE AERODYNAMIC STABILITY LIMIT

_____

THESIS

_____

A thesis submitted in partial fulfillment of the
requirements for the degree of Master of Science in
Mechanical Engineering in the College of Engineering
at the University of Kentucky

By:

Bradley D. Butler

Lexington, Kentucky

Director: Dr. Vincent R. Capece, Associate Professor of Mechanical Engineering

Paducah, Kentucky

2014

ABSTRACT OF THESIS

AXIAL COMPRESSOR FLOW BEHAVIOR NEAR
THE AERODYNAMIC STABILITY LIMIT

In this investigation, casing mounted high frequency response pressure transducers are used to characterize the flow behavior near the aerodynamic stability limit of a low speed single stage axial flow compressor. Time variant pressure measurements are acquired at discrete operating points up to the stall inception point and during the transition to rotating stall, for a length of time no shorter than 900 rotor revolutions. The experimental data is analyzed using multiple techniques in the time and frequency domains.

Experimental results have shown an increase in the breakdown of flow periodicity as the flow coefficient is reduced. Below a flow coefficient of 0.40 a two node rotating disturbance develops with a propagation velocity of approximately 23% rotor speed in the direction of rotation. During rotating stall, a single stall cell is present with a propagation velocity of approximately 35% rotor speed. The stall inception events present are indicative of a modal stall inception.

KEYWORDS: Turbomachines, Axial Compressor, Stall Inception, Modal Stall, Compressor Stability

Bradley D. Butler

4 April 2014

AXIAL COMPRESSOR FLOW BEHAVIOR NEAR
THE AERODYNAMIC STABILITY LIMIT

By:

Bradley D. Butler

Dr. Vincent R. Capece
Director of Thesis

Dr. James M. McDonough
Director of Graduate Studies

4 April 2014

ACKNOWLEDGMENTS

TABLE OF CONTENTS

LIST OF TABLES

LIST OF FIGURES

NOMENCLATURE

<u>Greek Symbols</u>

α Speed of sound

θ Transducer spacing

Θ Phase angle

ρ Density

Φ Flow coefficient

Ψ Pressure rise coefficient

Ω Rotational speed

<u>Latin Symbols</u>

A_c Compressor flow through area

B   Greitzer parameter

C   Chord length

CSC   Cross-spectrum correlation

C_x Inlet velocity

F   Force

FT   Fourier transform

i   Data point

k   Data points per revolution

L   Loadcell lever length

L_c Effective compressor duct length

LC   Loadcell

n   Number of nodes

N   Rotational speed

m	Number of revolutions
P	Pressure
P_{exit}	Exit static pressure
P_{Dev}	Flow periodicity breakdown
P_o	Stagnation pressure
P_{Rev}	Revolution pressure response
$\overline{P_{Rev}}$	Averaged revolution pressure response
P_{01}	Atmospheric pressure
R_{res}	Resistor resistance
R_{therm}	Thermistor resistance
S_{Rev}	Standard deviation for revolution pressure response
T	Temperature
T_o	Stagnation temperature
U_m	Mean blade speed
V	Plenum volume
V_e	Excitation voltage
V_o	Output voltage

1 INTRODUCTION

1.1 Background

The necessity to understand the fundamental problems associated with the design and operation of turbomachines becomes increasingly important as engineers strive to enhance turbomachinery performance. One of the challenges encountered in the design and operation of compressors for both commercial and military aircraft gas turbine engines is compressor stall. Not only does stall limit the operating range of compressors, but it will also induce large cyclic stresses that can lead to fatigue failures during operation.

As the pressure ratio increases and the mass flow rate is reduced, the compressor operating point moves closer to the stall inception point. At the stall line, schematically depicted in Figure 1-1 on a compressor operating map, compressor surge or rotating stall will occur. In some cases it is possible for both instabilities to occur as compressor surge can be initiated from a rotating stall. During surge the compressor experiences large amplitude fluctuations in the total annulus averaged mass flow rate at a relatively low frequency. When rotating stall is encountered, one or more stall cells are found to rotate around the circumference in the same direction as rotor blade rotation, but at a fraction of the rotational speed. Axial compressors used in aircraft gas turbine engines are designed to incorporate features to create a safety margin between the compressor operating line and the stall line.
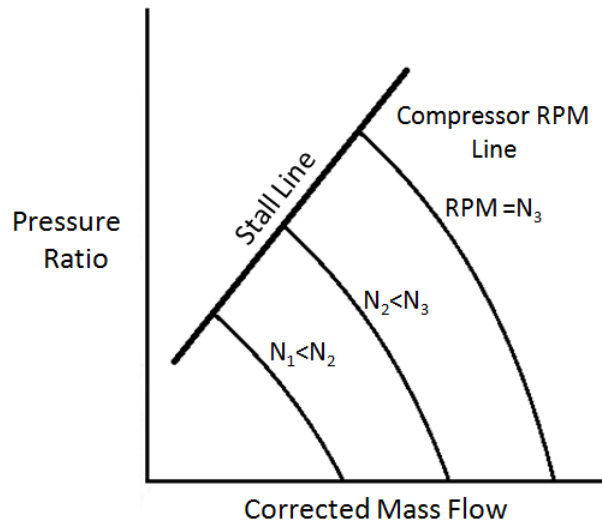
Figure 1-1: Typical performance map of a compressor at different operating speeds showing the stall line.

1.2 Literature Review

The development of analyses to understand and predict stall is an area of research interest. Due to the complexity of the flow field, including flow separation, and limitations in turbulence modeling, accurate prediction of stall has remained elusive. The literature in this area is voluminous and the following literature review focuses on papers that are directly related to the presented work.

The aerodynamic instability of surge was characterized by Greitzer (1981) with a relationship known as the Greitzer-*B* parameter as seen in Equation 1-1. Greitzer theorized that the stability of a pumping system could be determined through the use of rotor speed, speed of sound, plenum volume, compressor flow through area, and an effective length of the compressor duct. It was found that there is a critical value of *B* which determined whether the type of compressor instability experienced would be surge or rotating stall. Stenning (1980) demonstrated that in high pressure ratio compressors surge may be triggered very rapidly by a rotating stall and that the dip in the pressure rise caused by the rotating stall may be sufficient to induce surge. For low pressure ratio machines, like the University of Kentucky Low Speed Research Compressor (UKLSRC), Stenning showed that the compressors may not surge at all. The calculated Greitzer-*B* parameter value for the UKLSRC is estimated to be 0.08, which is well below the critical value for surge. The UKLSRC has been experimentally proven not to experience surge.

$$B = \frac{U}{2\alpha}\sqrt{\frac{V}{A_c L_c}} \qquad (1\text{-}1)$$

Two stall inception mechanisms have been identified with the first being previously defined theoretically for multistage compressors by Moore and Greitzer (1986), as a long wavelength axial velocity perturbation, sketched in Figure 1-2, which increases in amplitude until rotating stall develops as the compressor mass flow rate is decreased toward the stall point. This type of stall inception, which was first identified experimentally by McDougall et al. (1990) in a low speed compressor, is often referred to as modal stall. The small amplitude, long length scale, disturbances to the flow field can often be detected hundreds of rotor revolutions prior to stall inception. Modal stall is generally observed when the stagnation to static pressure rise characteristic has a zero or slightly positive slope at the stall line as demonstrated by Camp and Day (1998).
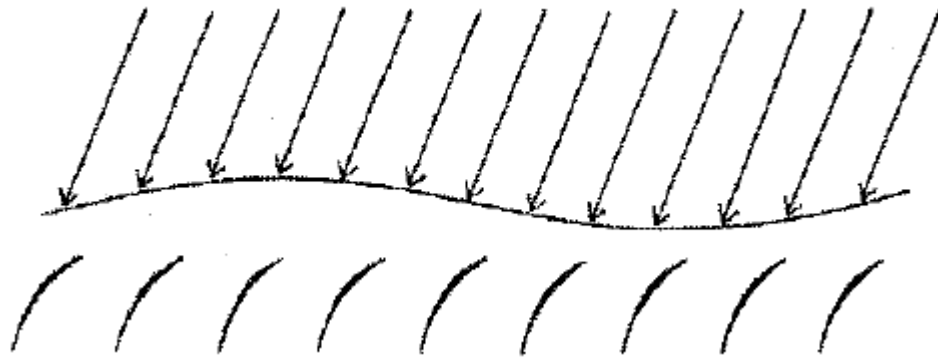
Figure 1-2: Sketch of a long wavelength axial velocity perturbation. Credit: Day (1993)

The second stall inception mechanism is a short wavelength disturbance, typically smaller than a few blade passages in size, which can be generated through a local flow separation that appears to be restricted to the tip region as shown by Day (1993). This stall inception gets the name 'spike' because any pressure measurement taken upstream of a developing disturbance will show an upward spike while velocity measurements will show a downward spike. Spike stall is found in compressors that feature a negative slope in the stagnation to static pressure rise characteristic at the stall line.

Recent research has also focused on resolving the breakdown of flow periodicity as stall is approached. Blade periodicity is how repeatable the blade passage response is from one revolution to the next and gives an indication to the amount of breakdown in the flow passage. An investigation by Young et al. (2011), while using a single stage low speed compressor, found an increase in the irregularity in the blade passage distribution as the compressor was throttled to stall. In the same investigation it was shown that the rotor tip clearance levels and eccentricity play a factor into the amount of unsteadiness and can greatly impact the flow coefficient for which a compressor stalls. Compressor eccentricity is quoted as the percentage of the average tip clearance size, an eccentricity of 200% would lead to blades rubbing the casing during operation at one circumferential location. For an eccentric compressor the area of minimum clearance is expected to be more stable than the area with the largest clearance. The tip clearances of the UKLSRC are smaller and more uniform than those studied by Young et al (2011).

1.3 Objectives

In this investigation, instrumentation, data acquisition, and data analysis procedures were established and used to investigate the stall inception characteristics of the University of Kentucky Low Speed Research Compressor (UKLSRC). The investigation utilized casing mounted high frequency response pressure transducers in different geometric configurations.

The overall objective of this research was to use the instrumentation configurations and data analysis procedures to investigate stall inception in a low speed axial flow compressor. The specific objectives were to utilize the detailed measurements of the time-variant pressure flow field in the rotor casing region to quantify the developmental features of rotating stall. In doing so, the breakdown of flow periodicity as the flow coefficient is reduced was investigated along with the development of structured disturbances in the casing endwall region. This work was directed towards furthering the understanding of compressor stall inception.

This facility has all of the capabilities necessary to experimentally investigate stall inception.

2   EXPERIMENTAL FACILITY

2.1   Facility Description

The experimental program was conducted in the Fred Paxton Engineering Research Center on the campus of West Kentucky Community and Technical College in Paducah, Kentucky. The building is the home to the University of Kentucky Low Speed Research Compressor (UKLSRC) as seen from the second floor in Figure 2-1. The facility is capable of experimentally evaluating the aerodynamic operation of an axial compressor.
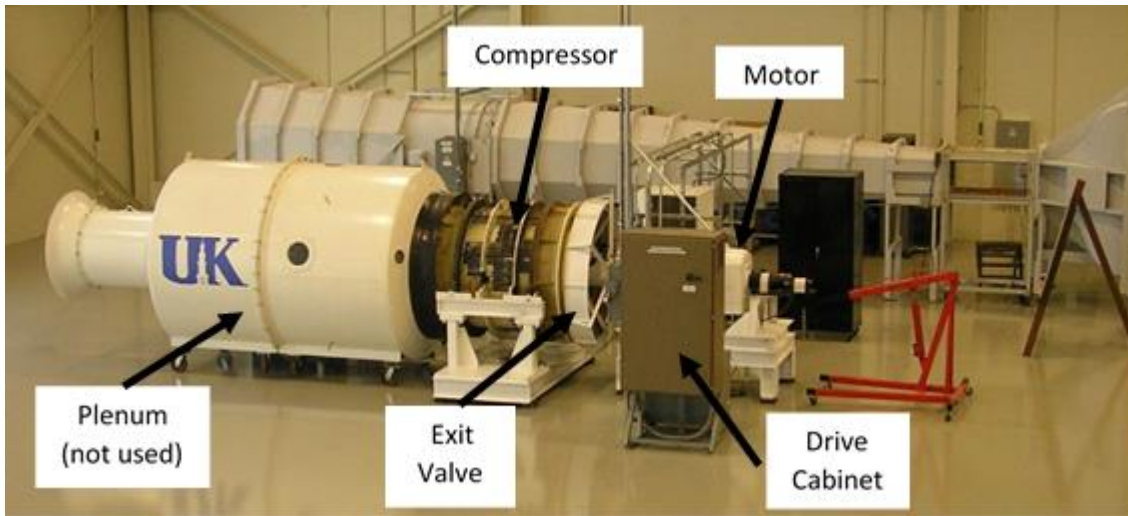
Figure 2-1: View of the UKLSRC from the second floor of the Fred Paxton Engineering Research Center.

The air used by the facility is the ambient room air without any filtration or treatment. Due to the large ceiling height of the research facility, the compressor is run prior to the acquisition of data until the temperature of the room has reached equilibrium. A 50 horsepower DC electric motor with tachogenerator feedback is used to provide stable rotational speeds. The flow exits from the test section radially and the mass flow rate through the compressor is controlled by a motorized valve in the exit plane which acts as a throttling valve.

Conventional steady state instrumentation, shown in Figure 2-2, was utilized to measure the inlet and exit flow fields and to define the compressor operating map. The test section inlet velocity profile, 2.2 rotor tip chord lengths upstream of the rotor blades, was determined with six equal circumferentially spaced eleven element total pressure rakes plus eight hub and casing static pressure taps. The instrumentation capability exists to measure the rotor exit flow field using a ten-element total pressure rake and a ten-element

temperature rake mounted on the leading edge of two adjacent stator vanes. The exit flow field downstream of the stator vanes was measured using seven eleven-element total pressure rakes along with hub and casing static pressure taps. Also, additional static pressure taps are located on the casing wall of one stator passage to quantify the stator vane tip static pressure distribution.
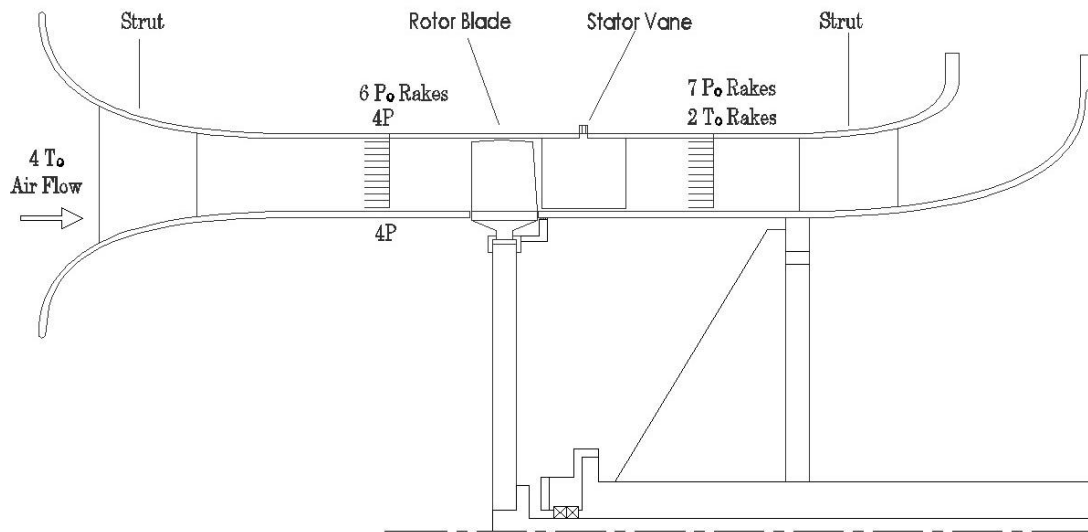
Figure 2-2: Flow path and conventional instrumentation schematic of the UKLSRC.

Time-variant data from high frequency pressure transducers and other instrumentation were acquired using National Instruments analog to digital converters. The digital data acquisition system was coded in MATLAB and all data was stored onto a hard drive for future review and post-test analysis.

The UKLSRC is fully instrumented and capable of taking the detailed flow measurements needed to research stall inception.

2.2   Test Article

In this study the stall inception of UKLSRC is considered, Figure 2-3. The compressor is a fully instrumented single stage axial flow machine whose design reflects the loading levels, geometry, and loss levels of the aft stages of a multistage compressor. The test section has constant tip and hub diameters, with a hub/tip radius ratio of 0.80. The large size of the compressor, with a casing diameter of 1.22 m, permits large quantities of instrumentation to be utilized for the quantification of the fundamental flow physics.
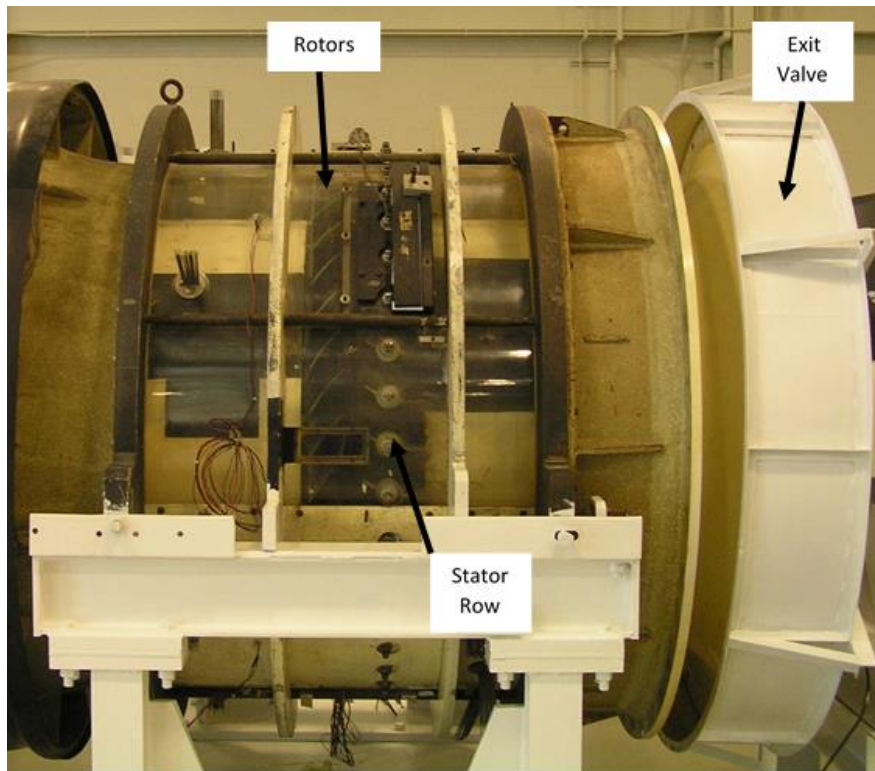
Figure 2-3: Side view of the UKLSRC.

The 42 rotor blades and 40 stator vanes have aspect ratios of approximately 1 and are based upon the NACA 65 series airfoil design. The airfoil mean section characteristics and compressor design point condition are given in Table 2-1. The rotor and stator airfoil designs have large camber angles in the hub region. The rotor blades have a maximum thickness of 7% of the chord at the hub that varies linearly to 4% of chord at the tip. The rotor blade chord also tapers linearly from hub to tip resulting in a solidity of nearly 1.6 at the hub and 1.3 at the tip. The stator vane has a constant thickness distribution from hub to tip with a solidity varying from 1.68 at the hub to 1.35 at the tip. The rotor blades and stator

7

vanes are made of fiberglass material molded around a steel spar that passes through the airfoil.

Table 2-1: Operating conditions at the design point and mid-span properties of the UKLSRC. Credit: Fleeter et al. (1980)

	Rotor	**Stator**
Airfoil Type	NACA 65 Series	NACA 65 Series
Number of Airfoils	42	40
Chord, c, (cm)	11.40	12.93
Solidity, c/s	1.435	1.516
Camber, Θ	20.42°	48.57°
D-factor	0.45	0.41
Aspect Ratio, s/c	1.046	0.943
Mean Blade Speed, U_m (m/s)	57	
Rotor-Stator Axial Spacing, (cm)	3.772	
Flow Rate, (kg/s)	14.07	
Design Rotational Speed, RPM	876.3	
Number of Stages	1	
Design Pressure Ratio	1.0125	
Inlet Tip Diameter, (m)	1.22	
Hub/Tip Radius Ratio	0.80	
Stage Efficiency, (%)	88.1	

The mean rotor blade tip clearance normalized by the rotor blade tip chord is 0.69% and when normalized by the annulus height is 0.64%. More detailed statistics of the rotor blade clearances at selected circumferential locations is illustrated in Figure 2-4. The statistics were generated by measuring the rotor tip clearance using feeler gauges with an uncertainty of 0.01 mm along the entire chord length at each designated circumferential location for each of the rotor blades. The compressor features an eccentricity of 43%.
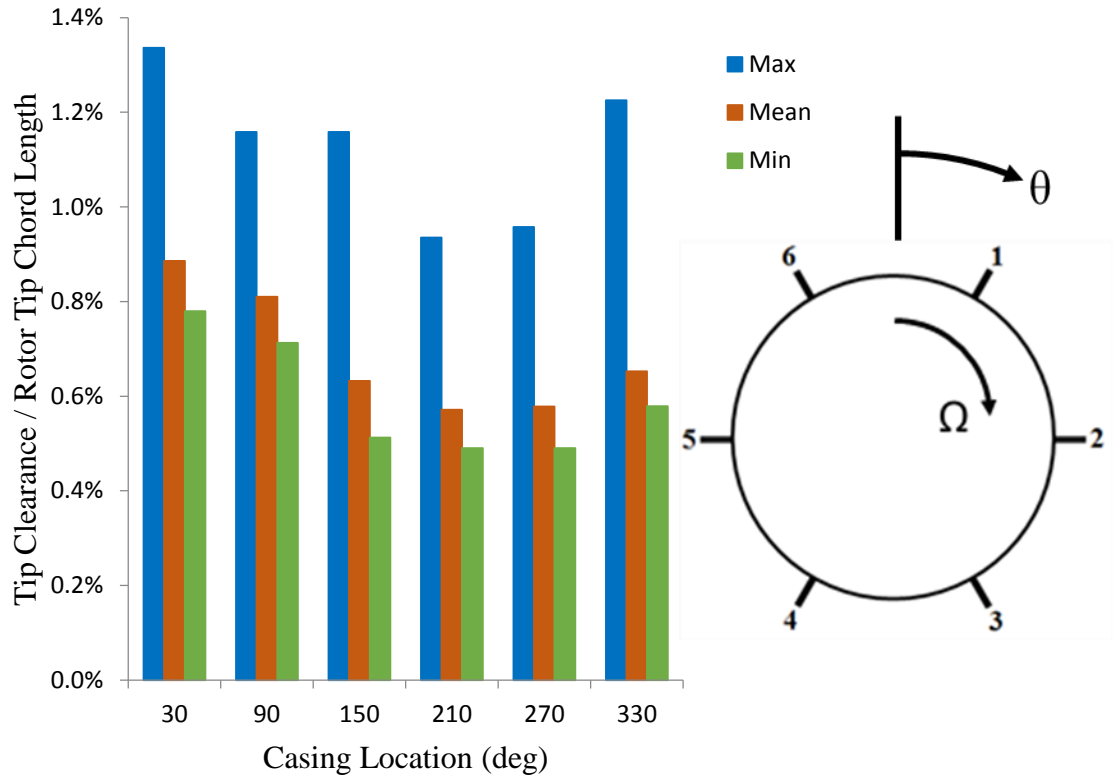
Figure 2-4: Non-dimensional tip clearances at selected circumferential casing locations.

2.3   Instrumentation

The following section outlines the instrumentation that the UKLSRC has been outfitted with for performance measurements and stall inception characterization.

2.3.1   Pressure Measurements

The UKLSRC is outfitted to measure dynamic pressures with high frequency response pressure transducers. The steady state pressures are measured with a digital pressure scanning array. Details of the pressure measurement instrumentation and calibration are in the following sub-sections.

2.3.1.1   High Frequency Response Pressure Transducers

High frequency response pressure transducers were used to measure the time variant pressures occurring within the UKLSRC. Kulite Miniature Ruggedized Pressure Transducers (XT-190 Series) were chosen to capture the unsteady pressure data; the specifications are listed in Table 2-2. The transducers were chosen because they are statically and dynamically capable with a natural frequency exceeding the data acquisition sampling rate. The transducers are, while being small in size, capable of being flush mounted to the casing or hub walls.

Table 2-2: Kulite Miniature XT Pressure Transducer Specifications. Credit: Kulite (2014)

Input Pressure Range	35 kPa
Diameter	3.8 mm
Input / Output Impedance	1000 Ohms
Natural Frequency	150 kHz
Acceleration Sensitivity % FS/g Perpendicular	1.5×10^{-3} FS/g
Operating Temperature Range	-55°C to 175°C
Weight	4 grams excluding cabling

The UKLSRC has three different base configurations for the pressure transducer locations. The first configuration has the transducers evenly spaced circumferentially around the casing over the rotor leading edge with a spacing of 60° between transducers, schematically depicted in Figure 2-5. The second configuration features the pressure transducers equally spaced along the rotor chord length in an aluminum insert to the casing. The aluminum insert has been machined such that the inside surface is flush with the casing and matches the radius of the compressor inner casing. The insert, schematically depicted

in Figure 2-6, has ten equally spaced locations from 17% rotor tip chord upstream of the leading edge to 33% rotor tip chord downstream of the trailing edge. The third configuration features five equally spaced locations on the casing that are across one rotor pitch of roughly 8.6°, depicted in Figure 2-7. Additionally, a pressure transducer was installed into the hub of the compressor, 40% rotor tip chord upstream of the leading edge, so spanwise disturbances can be quantified.
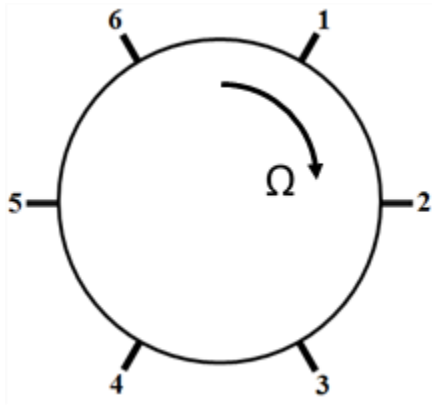
Figure 2-5: Schematic depiction of pressure transducer locations equally spaced circumferentially in the casing, over the rotor blade leading edge.
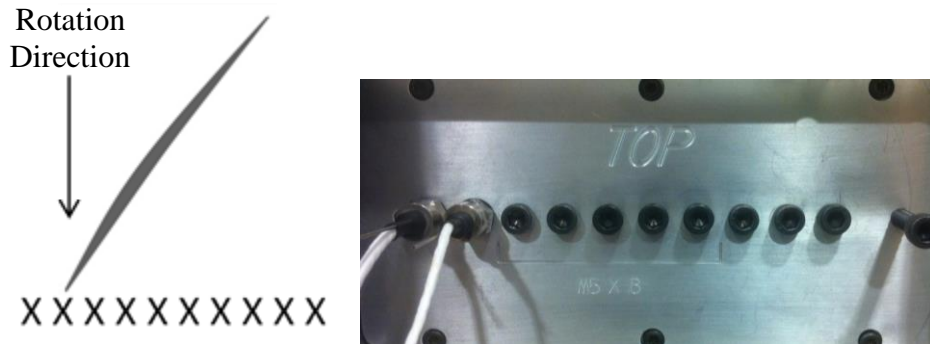
Figure 2-6: Representation of axial pressure transducer locations in the aluminum insert on the left, with a photograph of the aluminum insert shown on the right.
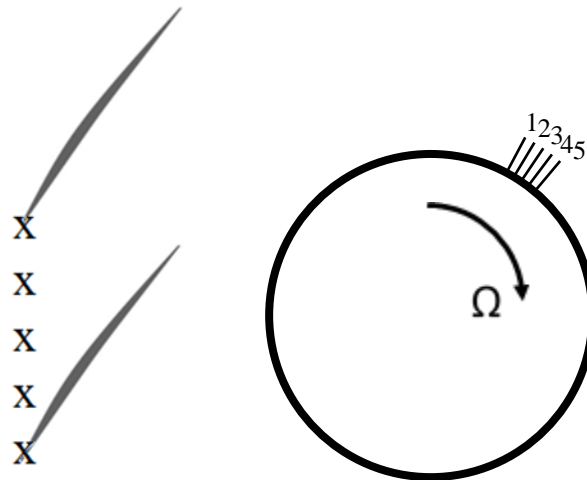
Figure 2-7: Illustration of the pressure transducer spacing across one rotor blade pitch at the leading edge.

The pressure transducers' outputs are in the low millivolt range so Omega OM5-WMV amplifiers were used to amplify the signal going into the data acquisition unit. The amplifiers have a gain of 50 with a quoted output accuracy of 0.08%. The amplification values were verified using a signal generator to generate a sine wave at various frequencies. A Fourier Transform was applied to the amplified signal to compare to the pre-amplified voltages. Figure 2-8 shows a slight trailing in amplitudes past 630 Hz, but it is less than 0.2%. Channel to channel comparisons of amplitude ratio and phase angle are shown in Figure 2-9 for all of the data acquisition channels with amplifiers. For the amplified channels the phase difference is less than 0.5° under 100 Hz and negligible in the range of interest.
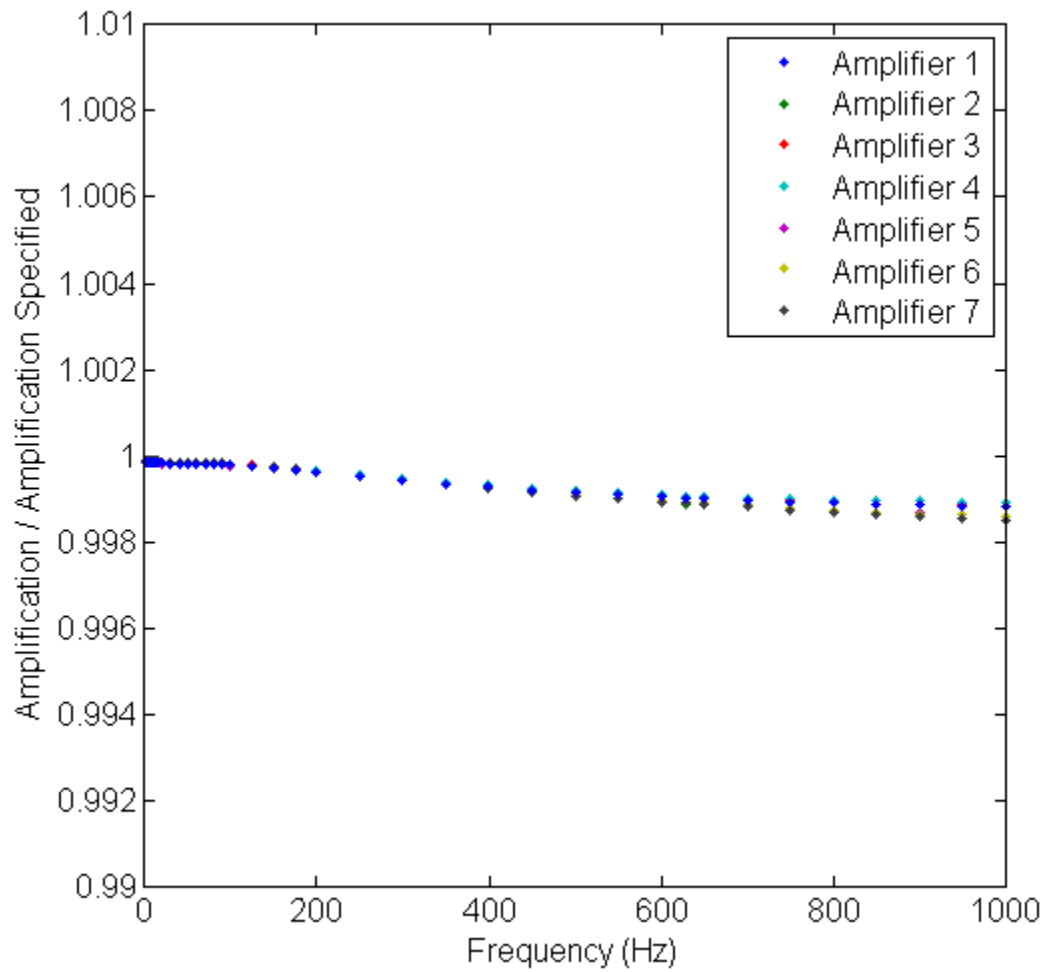
Figure 2-8: Amplification verification for amplifiers from 0 to 1000 Hz.
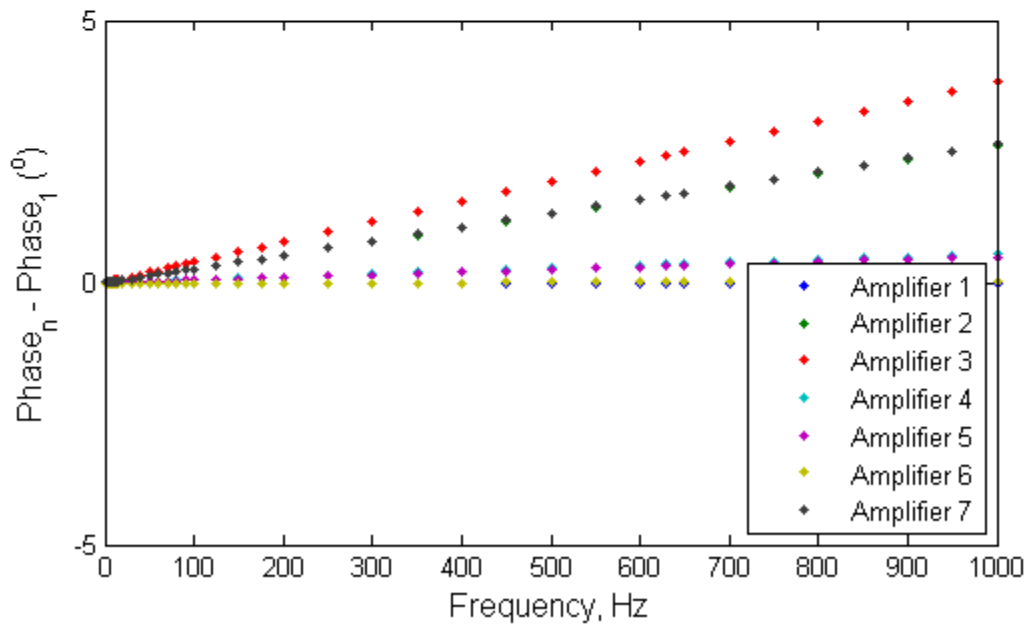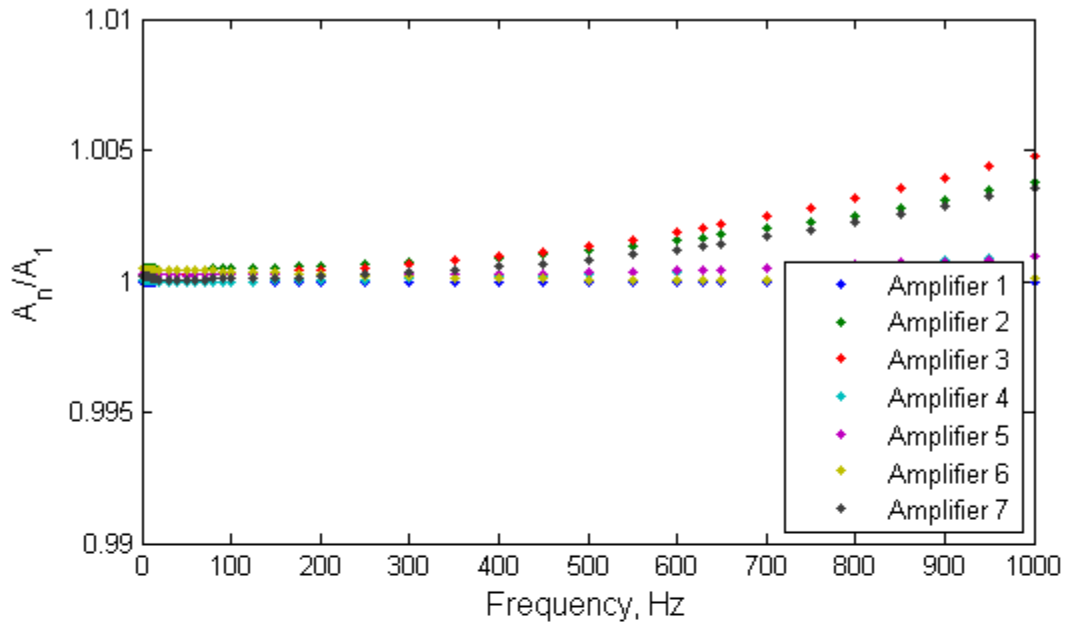
Figure 2-9: Channel to channel magnitude and phase variations for A/D converters and amplifiers used for dynamic pressure transducers.

2.3.1.2 Steady State Pressure Measurements

For measuring the steady state static and stagnation pressures, a digital pressure scanning array was used. The digital sensor arrays were manufactured by Scanivalve and are model DSA3016, which fit inside of the DSAENCL4000 enclosure. Two arrays are available with the first having a full scale pressure range of 2.5 kPa and the second of 6.9 kPa. Each array has 16 pressure channels for a total of 32. The array features a 16 bit A/D converter, which has a maximum sampling rate of 625 samples/channel/second, and communicates with the data acquisition computer with TCP/IP protocol.

2.3.1.3 Pressure Calibration

The Kulite pressure transducers and Scanivalve calibration procedure consists of taking one minute samples using a pressure vessel and water manometer with an error of ±0.002 psi. A calibration rig was constructed, schematically depicted in Figure 2-10, in which the pressure transducers could be properly secured and tested in along with the Scanivalve pressure scanner. The calibration technique applied the pressure to the sensing surface of the pressure transducers and to each port on the Scanivalve at the same time, so both systems could be compared to the water manometer reading. The calibration curves for the pressure transducers are shown in Figure 2-11.
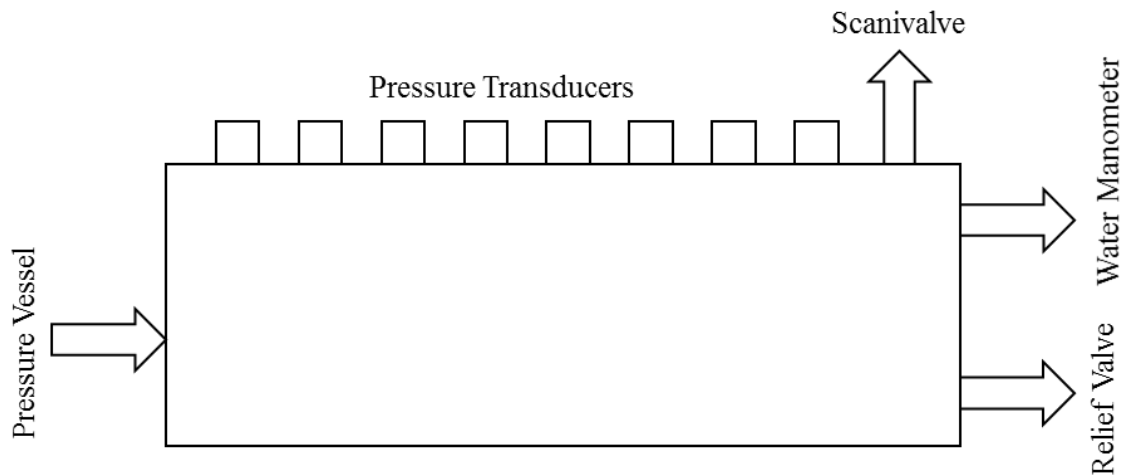
Figure 2-10: Pressure calibration rig schematic.
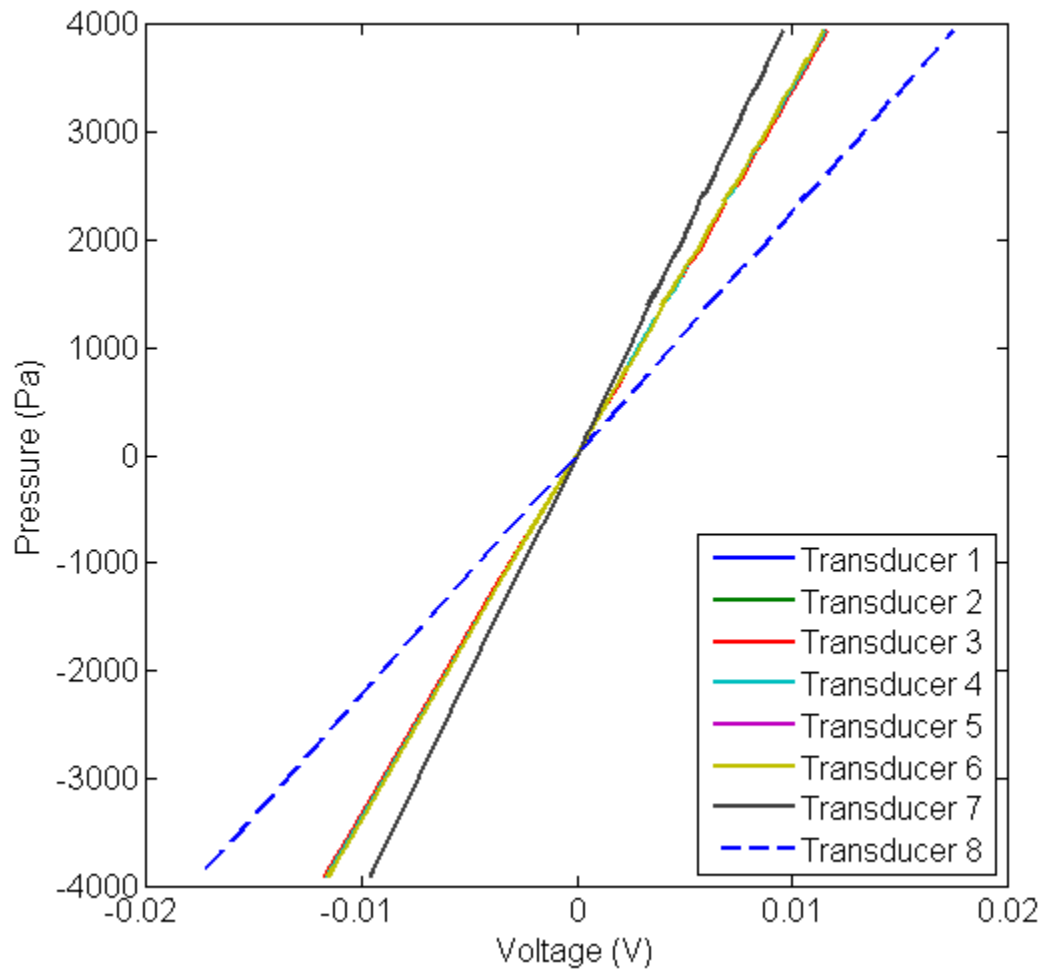
Figure 2-11: Kulite pressure transducer calibration curves.

2.3.2 Laser Tachometer

A laser tachometer, Monarch Instruments ROLS24-W, is positioned inside the hub region of the bell mouth inlet of the UKLSRC with wiring routed through a hollow support strut. It features a continuous laser that is rated for up to 250,000 RPM. The laser beam is mounted to provide a once per revolution pulse when rotor blade number 1 is at the top dead center of the compressor. This laser tachometer is powered with 8.5 Volts from the power supply and the output is fed into the data acquisition unit.

2.3.3 Loadcell

An Omegadyne loadcell, model LC101, is attached to the electric motor via a lever arm such that the loadcell is in tension and, as the motor turns, a torque is applied to the loadcell. A schematic for the loadcell configuration is shown in Figure 2-12. The amount of power is calculated using the deProny equation with a constant lever arm length, the rotational speed of the motor, and the force upon the loadcell, Equation 2-1 (Beckwith 2007).

$$Power = 2\pi L \cdot F \frac{N}{60} \tag{2-1}$$
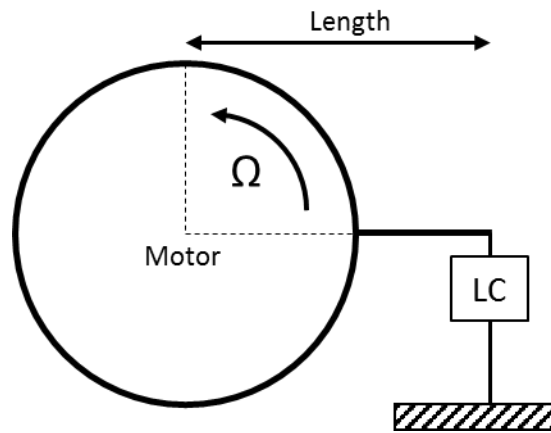
Figure 2-12: Schematic showing loadcell configuration as seen from the aft looking forward.

2.3.4 Thermistor

A thermistor is used to quantify the atmospheric temperature in the research bay. The thermistor is set up in a voltage divider circuit, shown in Figure 2-13, and given an input voltage, which is measured using the data acquisition system. The output voltage from the divider circuit is measured using the data acquisition system and the thermistor resistance is calculated using Equation 2-2 and is then used in Equation 2-3 (Beckwith 2007) for calculating the atmospheric temperature, where A, B, and C are supplied constants for the thermistor.

$$R_{therm} = V_o(\frac{R_{res}}{V_e - V_o}) \tag{2-2}$$

$$T = \frac{1}{A + B \log(R_{therm}) + C \log(R_{therm})^3} \tag{2-3}$$
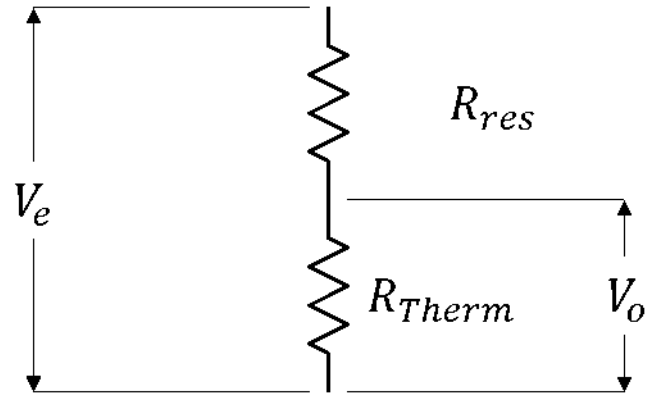
Figure 2-13: Voltage divider schematic used to measure thermistor resistance.

2.4 Experimental Procedure

Unsteady pressure measurements were acquired at discrete operating points up to the stall inception point and during the transition to rotating stall. For each discrete operating point, the compressor was given time to settle before data was acquired. Data was then acquired over a length of time no shorter than 900 rotor revolutions before the exit valve was moved to change the mass flow rate. In addition, the variable speed throttling valve was closed at a very slow speed and the unsteady pressure measurements were continuously recorded transiently as the compressor moves from the design point to fully developed rotating stall. A linear potentiometer attached to the exit valve quantifies the displacement of the exit valve from the wide open discharge condition.

3   DATA ACQUISITION AND ANALYSIS

3.1   Data Acquisition

Two types of data were acquired, steady state and time variant. The steady state section details the pressure measurements in the inlet and the exit flow field where the pressure was assumed to be steady with minimal rotor induced pressure fluctuations and was sampled at a relatively low sampling frequency. The time variant section details the measurements that were taken at a high sampling frequency.

For a given operating point the compressor was given time to stabilize from any transient effects of the exit valve being moved before data was acquired. The steady state and time variant data were acquired simultaneously. Data was acquired over a minimum duration of time of 60 seconds, which included 900 or greater rotor revolutions. The exit valve position was then adjusted and the data acquisition process was repeated.

3.1.1   Steady State

The inlet and exit flow field, static and stagnation pressures, are measured with the Scanivalve digital pressure scanning array that has an uncertainty of ±0.2% full scale. The pressures were sampled 250 times per second with the average pressure for each channel being reported. There were 30 reported values for each pressure channel per data set at a fixed operating point. The reported values were then averaged to provide a single pressure value for each of the measurement locations. The Scanivalve digital pressure scanning array connects to the data acquisition computer using a TCP/IP connection.

3.1.2   Time Variant

The time variant data was digitized using National Instruments A/D modules with each channel being sampled at 100k samples per second. This sampling rate allows the high frequency response transducers to acquire detailed measurements of more than 150 points per rotor blade passage at the design rotational speed. The laser tachometer and loadcell were also sampled at the 100k samples per second sampling rate.

3.2   Acquisition Program

In the early stages of this investigation, the data was being acquired using the National Instruments LabVIEW program for the time variant data and by manually querying the steady state pressures from the Scanivalve pressure scanner. The time variant

19

data was being sampled at 50k samples per second, half of the maximum sampling rate, and at a reduced total number of channels. Data recording and storage issues arose after acquiring additional instrumentation which lead to the creation of a data acquisition program using MATLAB.

The data acquisition program was created with the use of the Data Acquisition Toolbox for MATLAB, and can be found in the Appendix. This allowed for sampling at the maximum possible rate, providing more points per blade passage, and for Scanivalve integration using TCP/IP protocols to automatically send commands and retrieve data. The data acquisition program runs in the background of MATLAB, continuously sampling the data, and begins writing the data to disk with the push of a button. The hardware configuration is schematically shown in Figure 3-1 including the data acquisition computer, pressure scanning system, and amplifiers. The current exit valve position in terms of percent closed is visible on screen to help in the setting of operating points allowing for fine adjustments in the near stall region.

K – Pressure transducers
L – Loadcell
O – Laser tachometer
P – Linear potentiometer
T – Temperature
A – Amplifier
NI – National Instruments
SV – Scanivalve
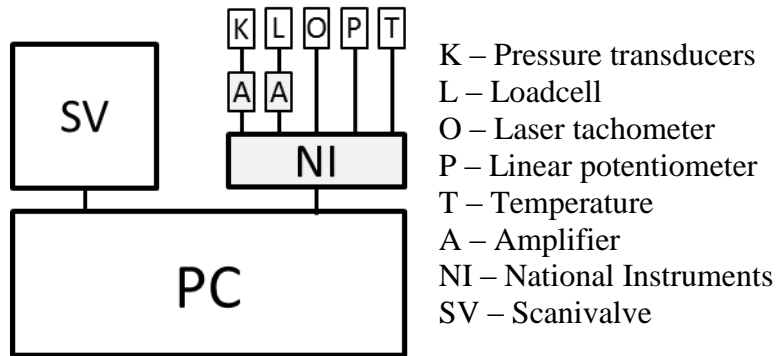
Figure 3-1: Data acquisition system schematic.

3.3 Data Analysis

The data analysis techniques used in this study to characterize the flow behavior of the UKLSRC are detailed in the following section. These techniques could also be applied to characterize the flow behavior of other turbomachines.

3.3.1 Steady State

The general behavior of any turbomachine can be obtained from dimensional analysis techniques. Buckingham Π theorem is a method for nondimensionalization by providing sets of dimensionless parameters from given key variables. A non-dimensional quantity can be formed, called the flow coefficient, which is calculated by comparing the

axial velocity to the mean blade speed as seen in Equation 3-1 and has a maximum margin of error of 3.4%. The pressure rise in a low speed compressor can be characterized by using the non-dimensional pressure rise coefficient. The pressure rise coefficient seen in Equation 3-2 compares the total static pressure rise to the mean dynamic pressure and has a maximum margin of error of 2.0%. Comparing the flow coefficient to the pressure rise coefficient produces a plot of the compressor characteristics. Due to the non-dimensionality of the parameters all rotational speeds will collapse into a single curve but Reynolds number effects can become dominate at the stall inception point. The Reynolds number based off rotor tip chord length at design speed is near 410000 and Reynolds number effects near stall are small.

$$\Phi = \frac{C_x}{U_m} \tag{3-1}$$

$$\Psi = \frac{P_{exit} - P_{01}}{\frac{1}{2}\rho U_m^2} \tag{3-2}$$

3.3.2 Time Variant

The following sub-sections explain the data analysis techniques that were applied to the time variant pressure measurements.

3.3.2.1 Flow Deviations

Flow periodicity is the repeatability of the pressure profile of a rotor passage to be the same between revolutions as illustrated in Figure 3-2 and periodic from passage to passage. The breakdown of flow periodicity leads to irregularities in the blade passing signature. The impact of these irregularities can be measured by looking at the standard deviation of the flow compared to a mean value. The laser tachometer was used as an indicator of each rotor revolution and was used to split the time domain pressure transducer signals into a series of revolutions. Each revolution was linearly interpolated to account for minor differences in the rotational speed. The mean pressure profile was determined by averaging all of interpolated pressure profiles to achieve a single profile from which the standard deviation was then calculated for each point across the blade passage through use of Equation 3-3 and 3-4, respectively. The deviation was calculated for each revolution as a whole and then for each blade passage between the pressure and suction surfaces, which does not include the pressure jump over the thickness of the blade. The mean of the

21

standard deviations, Equation 3-5, was used as a method of quantifying the breakdown of flow periodicity. An example of what the mean pressure profile and flow deviation bands would look like is shown in Figure 3-3.

$$\overline{P_{rev,\iota}} = \frac{1}{m} \sum_{Rev=1}^{m} P_{Rev,i} \tag{3-3}$$

$$S_{Rev,i} = \sqrt{[\frac{1}{m-1} \sum_{Rev=1}^{m} (P_{Rev,i} - \overline{P_{Rev,\iota}})^2]} \tag{3-4}$$

$$P_{Dev} = \frac{1}{k} \sum_{i=1}^{k} S_{Rev,i} \tag{3-5}$$
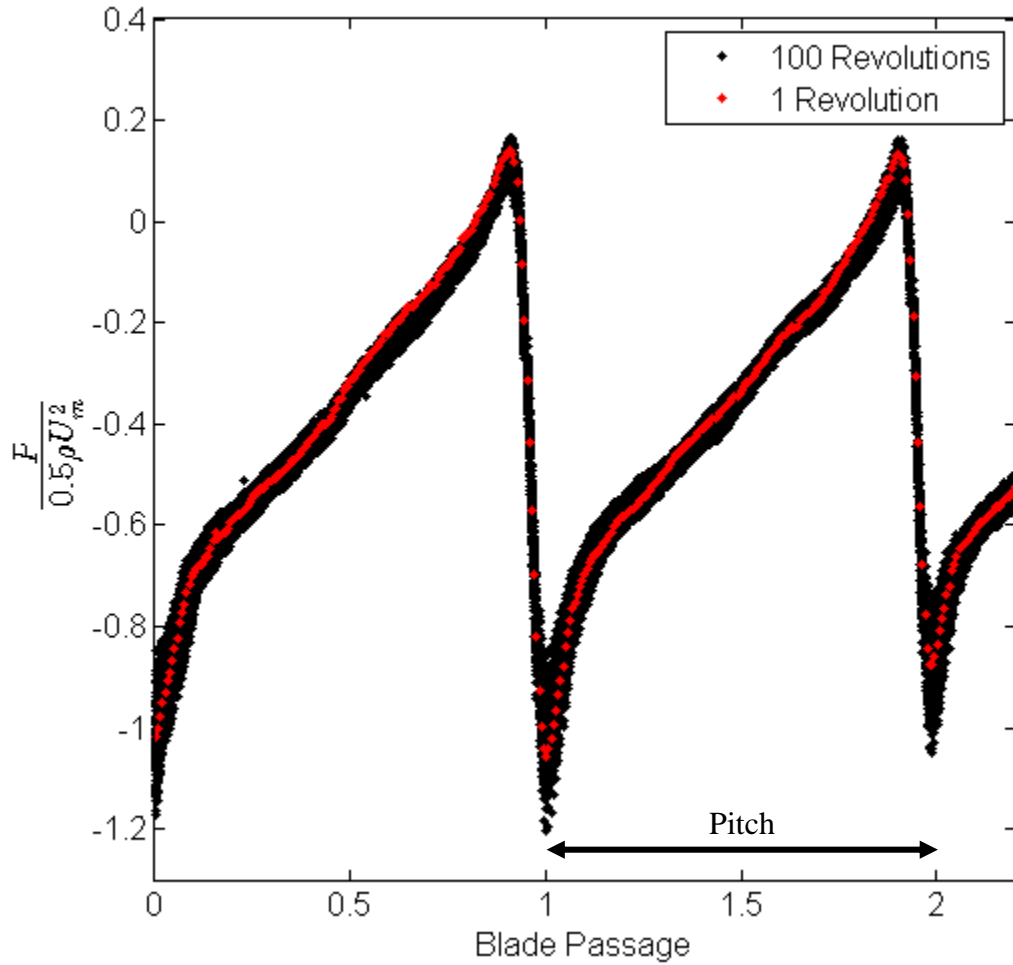
Figure 3-2: Flow periodicity example showing the data scatter for 100 rotor revolutions.
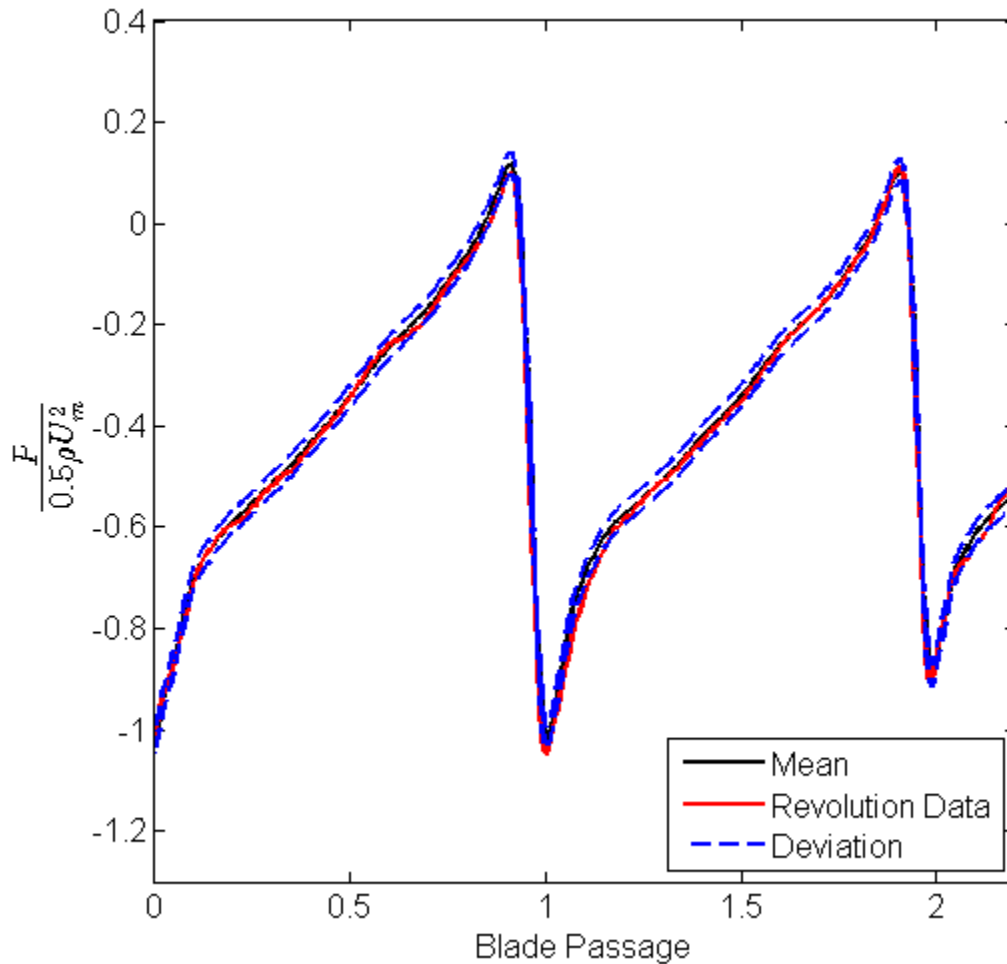
Figure 3-3: Example flow deviation showing the mean pressure profile and data points from a single revolution.

3.3.2.2 Cross-Spectrum Correlations

To determine the number of coherent cells in a rotating disturbance, it is necessary to perform a cross power spectral analysis between two pressure transducers. Figure 3-4 demonstrates the calculation of the cross power spectrum between two transducers 60° apart in the rotor leading edge plane. The cross power spectrum was computed by multiplying the Fourier transform of one transducer by the conjugate of the Fourier transform of the second transducer, Equation 3-6. To compute the number of coherent nodes at a given frequency in the cross-power spectrum, the phase at the frequency was divided by the angular separation between the two transducers, Equation 3-7. The number of nodes represents the number of complete sine waves around the annulus.

$$CSC = FT_1 \cdot conjugate(FT_2) \qquad\qquad (3\text{-}6)$$

$$n = \frac{\phi}{\Delta\theta} \qquad\qquad (3\text{-}7)$$
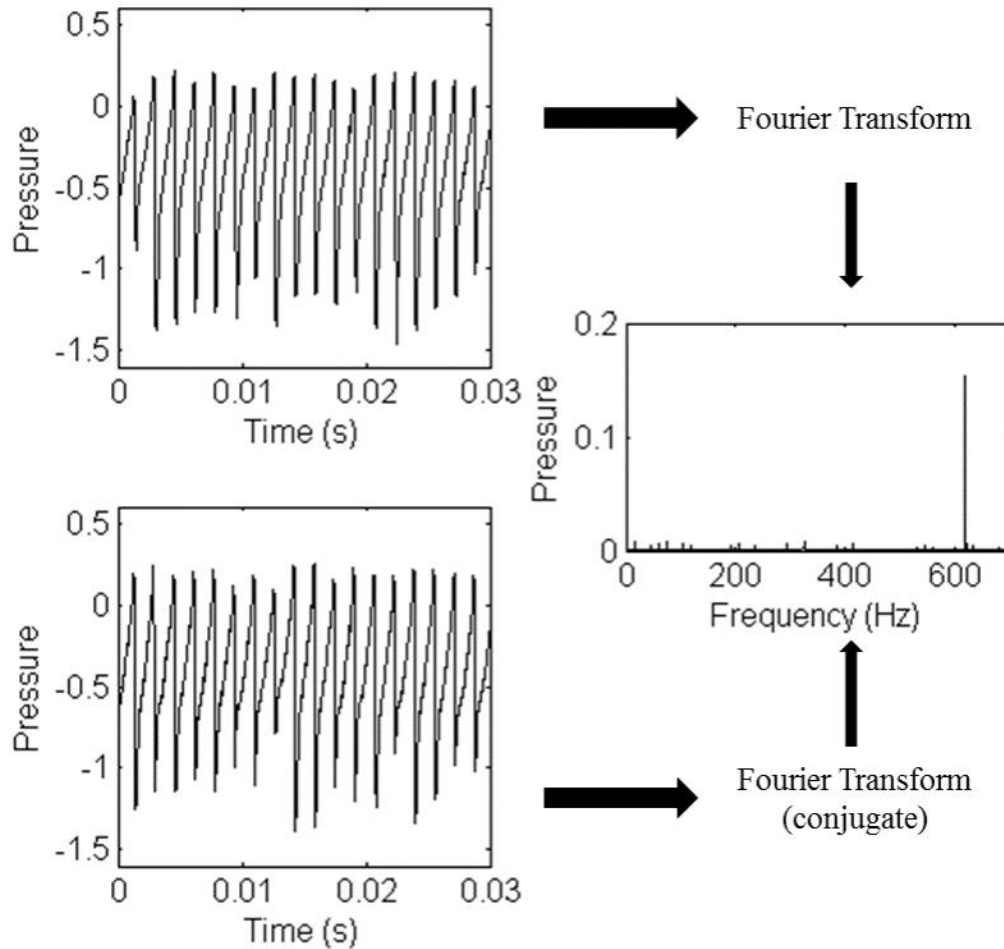
Figure 3-4: Procedure for calculating cross-spectrum correlation. The top left figure is pressure transducer 1, and the bottom left figure is pressure transducer 2. The Fourier transform for transducer 1 is multiplied by the conjugate of the Fourier transform for transducer 2.

3.3.2.3 Filtering

To observe pressure fluctuations in the near stall inception region that are less than the rotor passing frequency, a filter was applied to the pressure transducer signal. The filter used was a low-pass fourth order Butterworth filter. To remove the blade passing component, the cutoff frequency was chosen to be half the rotor blade passing frequency

with a typical value of 315 Hz. Lower cutoff frequencies were used depending upon application.

3.3.2.4   Spatial Fourier Transform

To better understand the stall inception phase, the circumferential array of 6 equally space pressure transducers in the rotor leading edge plane was used. This method meets the requirements of capturing the time variant pressure field around the rotor at each instant in time. The circumferential pressure field was analyzed at each time step shown in Figure 3-5. The compressor has 42 rotor blades, which means 84 pressure transducers are required to avoid aliasing of the first 42 spatial waves. For this study, only 6 pressure transducers were available, meaning that aliasing will occur for any wavenumber greater than 3. A low-pass filter with a cutoff frequency of 9 Hz was used to condition the data due to the spatial limitations.
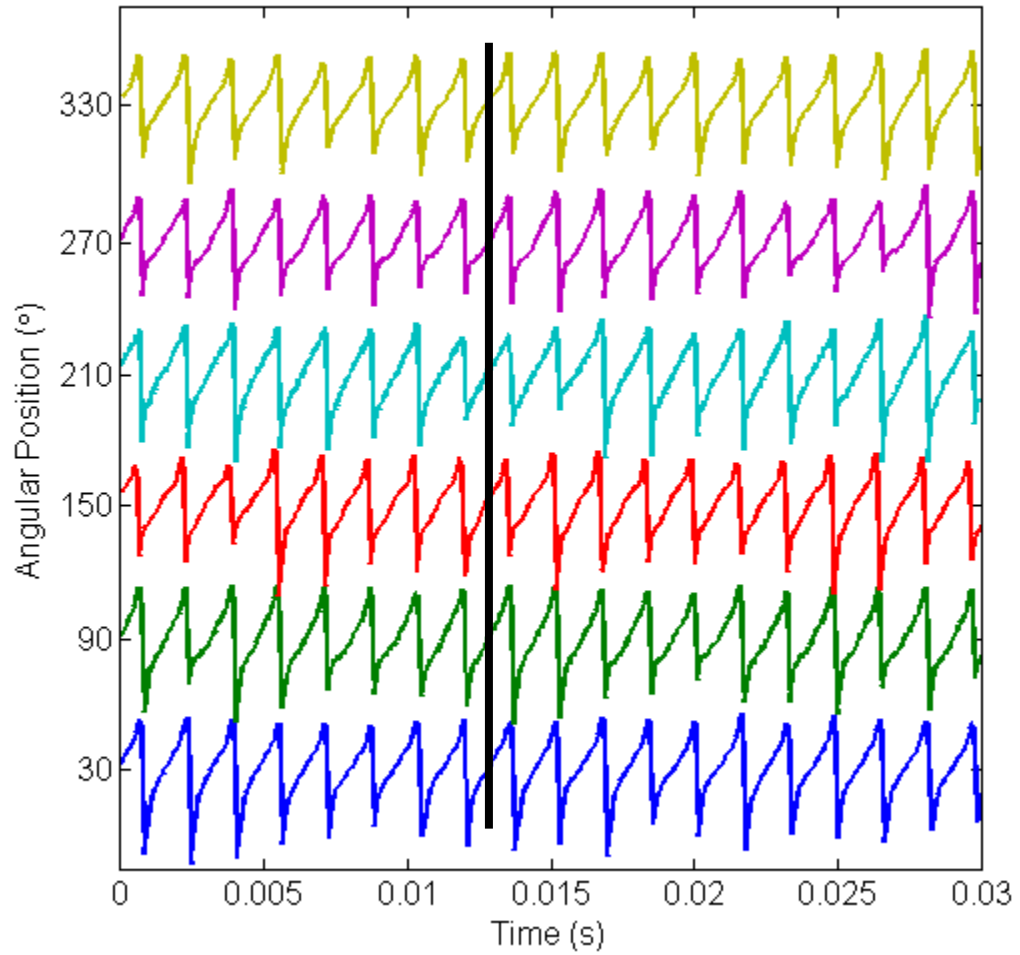
Figure 3-5: Visualization of each pressure transducer at the same time step. The signals have been offset for plotting purposes.

4   RESULTS

In this chapter the data analysis techniques presented in Chapter 3 will be applied to the different pressure transducer configurations. The following four key operating conditions of the compressor will be emphasized: design point, near stall inception, stall inception, and fully developed rotating stall. The operating conditions of the compressor at the design point are used as the basis for comparing the near stall inception and the fully developed rotating stall conditions.

4.1   Steady State Performance

A series of experiments were conducted to establish the steady state compressor characteristic as presented in Figure 4-1. Testing occurred at different rotational speeds to illustrate the dynamic similarity of the compressor at different operating speeds as shown by the operating points collapsing to form a single curve. The pressure rise coefficient increases rapidly with the decrease in flow coefficient as the compressor is initially throttled. As the stall point is approached, the pressure rise coefficient levels off and has a near zero slope at the stall inception point. The near zero slope of the compressor characteristic curve at the stall inception point is indicative of a modal stall inception.
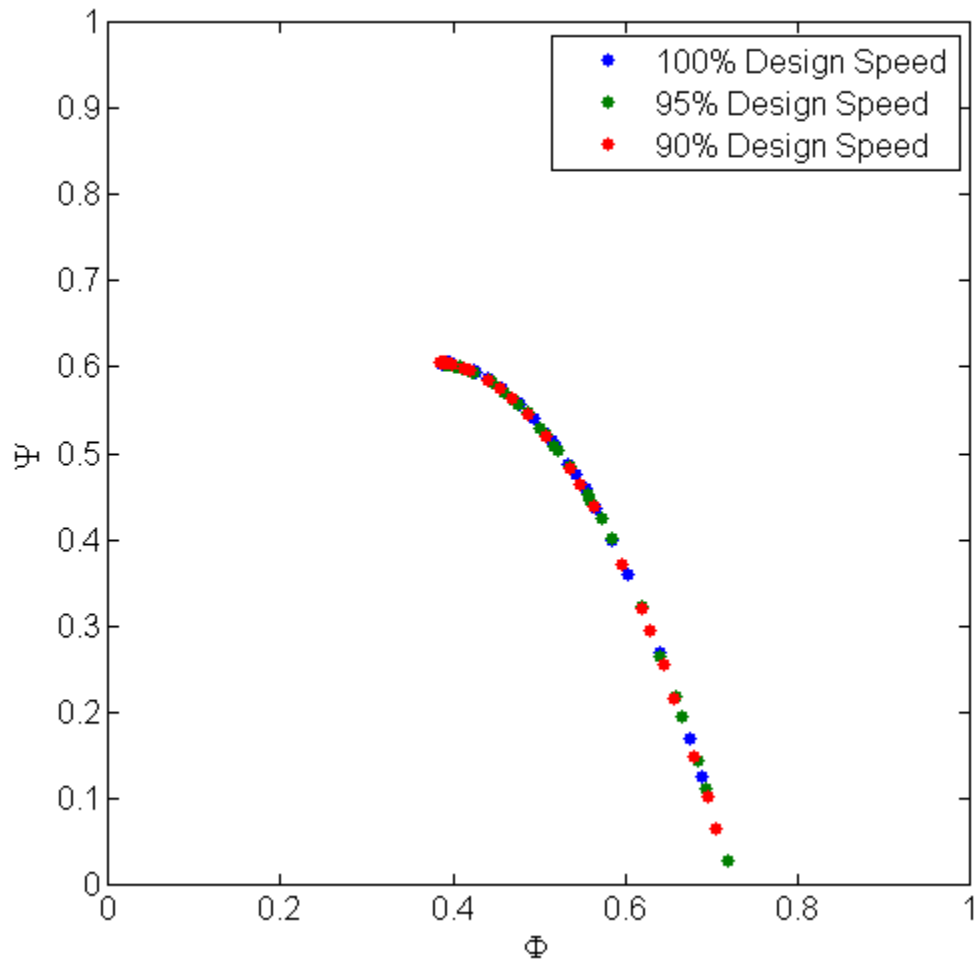
Figure 4-1: Overall compressor performance map.

The alternative to the non-dimensional compressor characteristic map is the pressure ratio operating map depicted in Figure 4-2, which compares the pressure ratio to the mass flow rate on various operating lines. The limiting stall line is generated by the stall inception points at the various operating speeds. The small exit valve closure adjustments, made possible by the sensitive exit valve motor controller, allowed for a more accurate stall inception point.
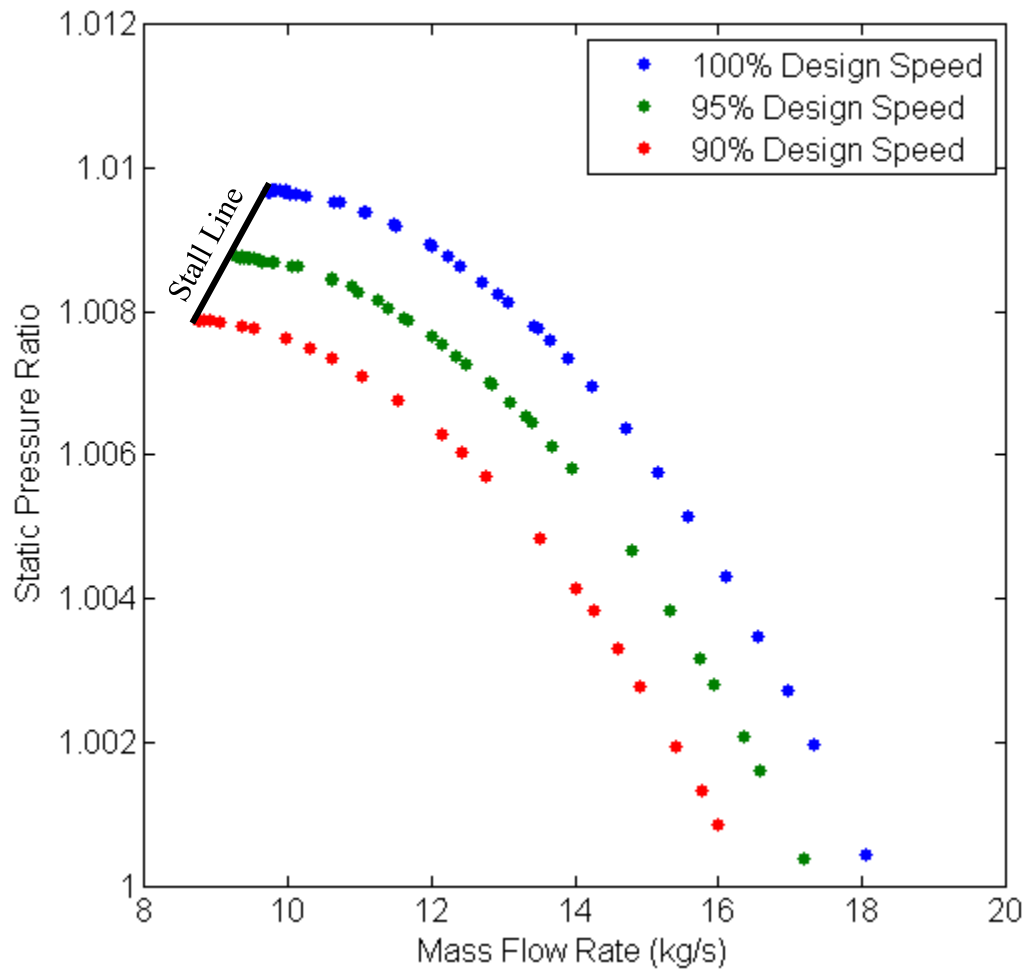
Figure 4-2: Static pressure ratio as a function of mass flow rate.

4.2 Time Variant

Results will now be presented that used the high frequency response pressure transducers to track the time variant pressures occurring inside of the compressor. The flow deviation measurements that track the amount of flow irregularity in the blade periodicity, Fourier analysis, and time traces will be presented using different pressure transducer configurations.

4.2.1 Equally Spaced Circumferential Pressure Transducer Configuration

4.2.1.1 Flow Deviations

The flow deviations for transducers in the circumferential configuration are illustrated in Figure 4-3. As the flow coefficient was decreased, the amount of irregularity in the blade periodicity increased in a monotonic fashion up to a flow coefficient of approximately 0.4. Additional throttling of the compressor induced a rotating disturbance that can be seen by the sharp increase in the irregularity of the flow prior to stall inception. The distribution of flow irregularities in the rotor leading edge plane was fairly uniform with no location experiencing a much larger amount than any other. When the pressure transducer located in the hub of the compressor is considered, the amount of change in flow irregularities was rather constant until the 0.4 flow coefficient region, in which a large increase was seen. The overall amplitude of the flow periodicity breakdown was less at the hub of the compressor due to being away from the tip clearance flow and 40% rotor cord upstream of the rotor leading edge.
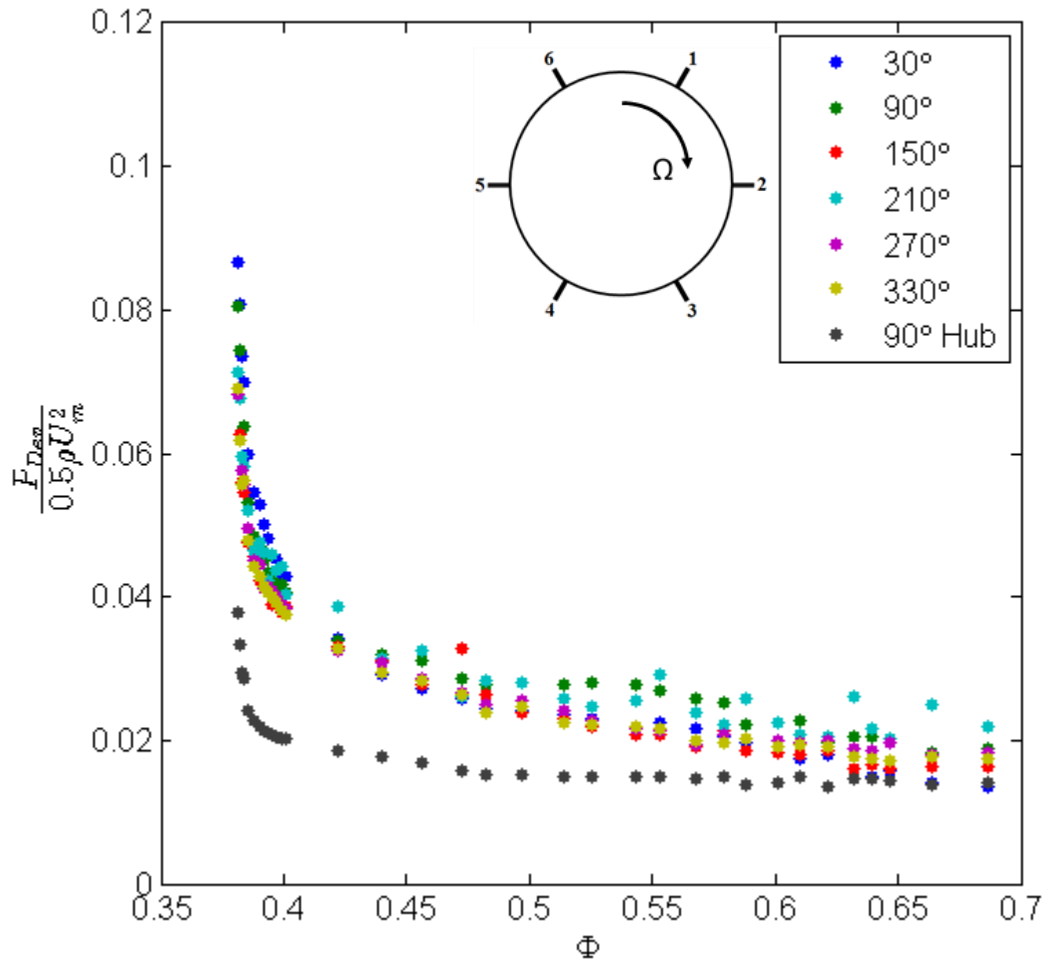
Figure 4-3: Blade periodicity deviations for the circumferential configuration in the rotor leading edge plane, except where denoted by hub.

4.2.1.2 Time Dependent Pressures

The time variant casing pressure measurements shown in this section have been treated with a low-pass filter to remove the pressure component due to blade passing. The time traces during fully developed rotating stall are shown in Figure 4-4. By tracing a line through the peak of the stall cell as it rotates about the annulus, a propagation speed and frequency can be determined that is around 5.2 Hz. It is also evident from visual inspection that a single stall cell exists.

To determine the speed of the rotating stall cell, Equation 4-1 is utilized, which relates the distance traveled by the cell to the time it takes to travel that distance. The distance the cell travels is calculated with Equation 4-2. The stall cell speed is then non-

dimensionalized by the mean blade speed to be presented in terms of percent of rotational speed. In Figure 4-4 it takes the stall cell denoted with the black line approximately 0.16 seconds to propagate from the 30° to 330° transducer locations. Implementing Equations 4-1 and 4-2 and non-dimensionalizing, the rotating stall cell speed is calculated to be 35% of rotor rotational speed.

$$v = \frac{\Delta x}{\Delta t} \tag{4-1}$$

$$\Delta x = \pi D \frac{\Delta \theta}{360} \tag{4-2}$$
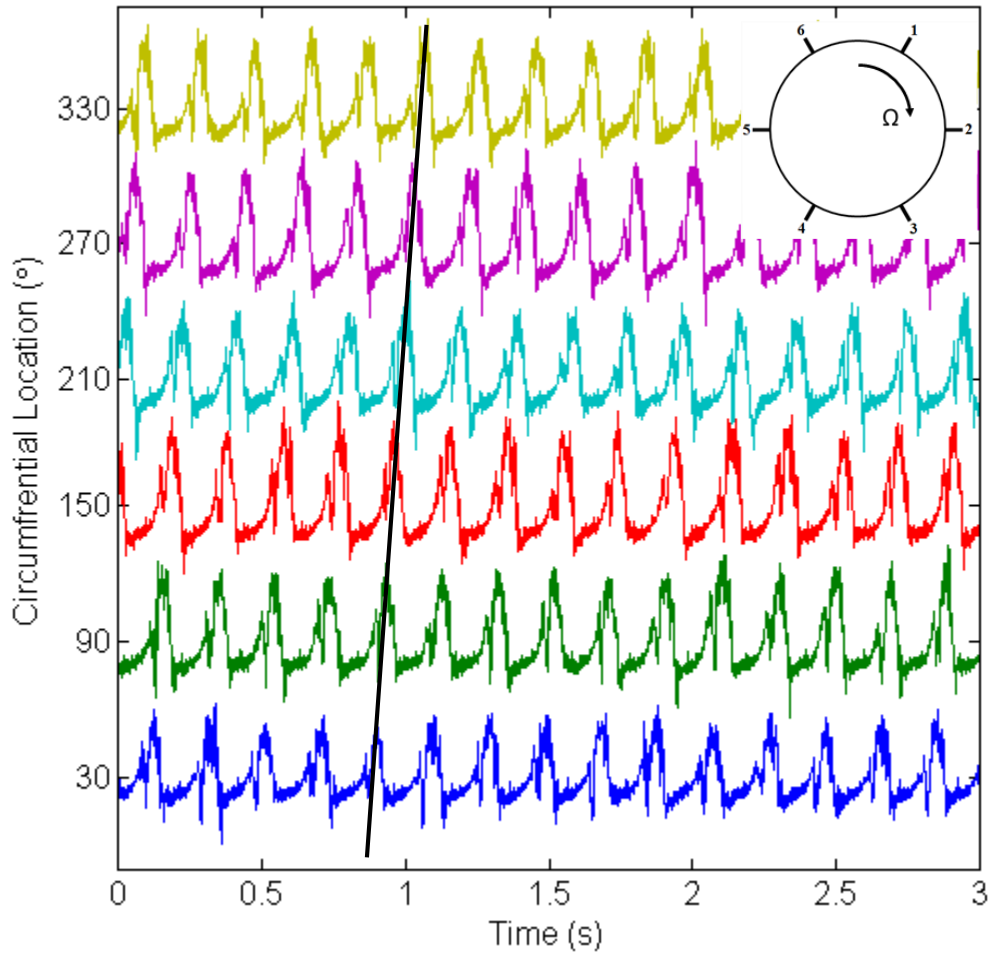
Figure 4-4: Filtered time trace showing the rotating stall cell pressure signal at leading edge circumferential locations.

This procedure can be repeated for a flow coefficient near the stall inception point. At a flow coefficient less than 0.4, a low frequency periodic disturbance is evident in the filtered pressure traces that occurs roughly 20 times over the three second interval shown in Figure 4-5. By drawing lines through the disturbance while it travels around the annulus a two node disturbance becomes apparent. The solid line represents the first node while the dashed line represents the second node. When processed using a standard Fourier transform, this disturbance has a frequency of roughly 6.8 Hz. Repeating the calculations done for the rotating stall case, Equations 4-5 and 4-6, the pre-stall disturbance is found to travel near 23% rotor rotational speed.
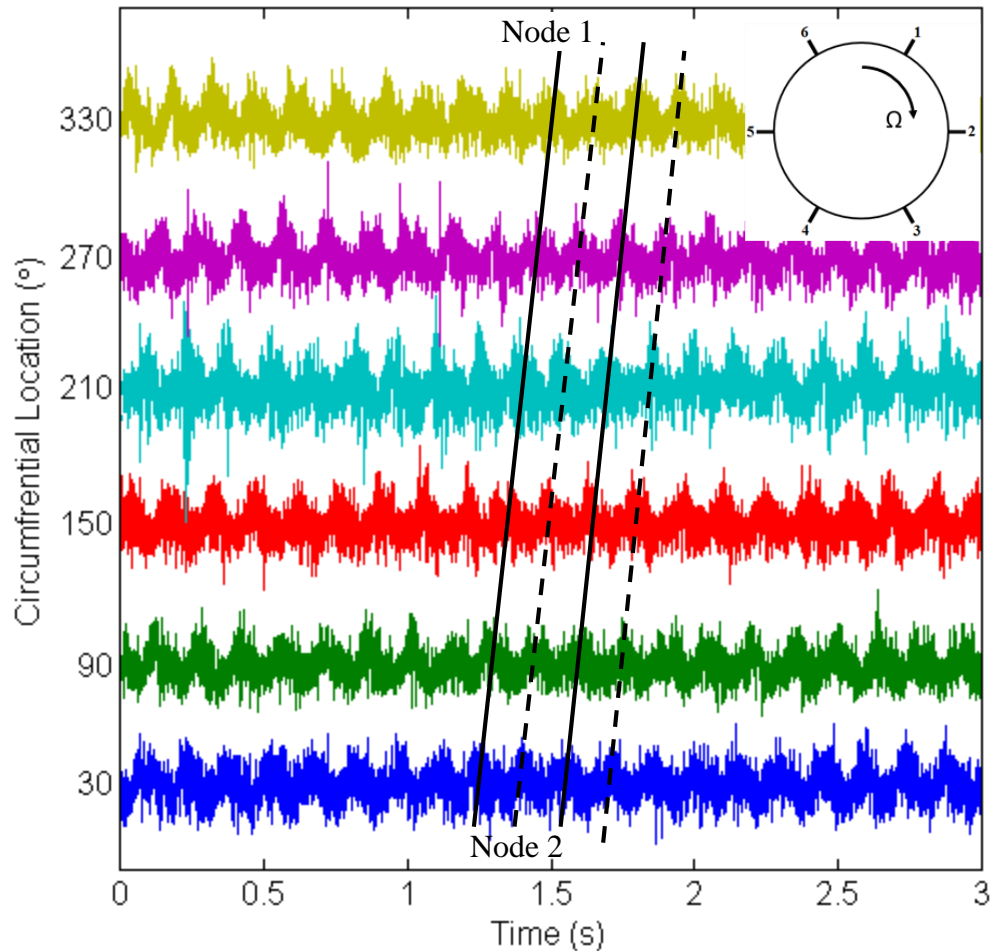
Figure 4-5: Filtered time trace showing the pre-stall disturbance pressure signal at circumferential locations.

This periodic pre-stall disturbance will eventually reach a critical condition and stall will be initiated in the compressor. A stall inception event can be seen in Figure 4-6, which shows the pre-stall disturbance at 0 seconds with the stall initiation occurring near 1.5 seconds and the mature stall cell being seen before the 3 second mark. The stall cell rapidly grows from the inception event that occurs at about 1.5 seconds at the 210° transducer location into a fully developed rotating stall cell.
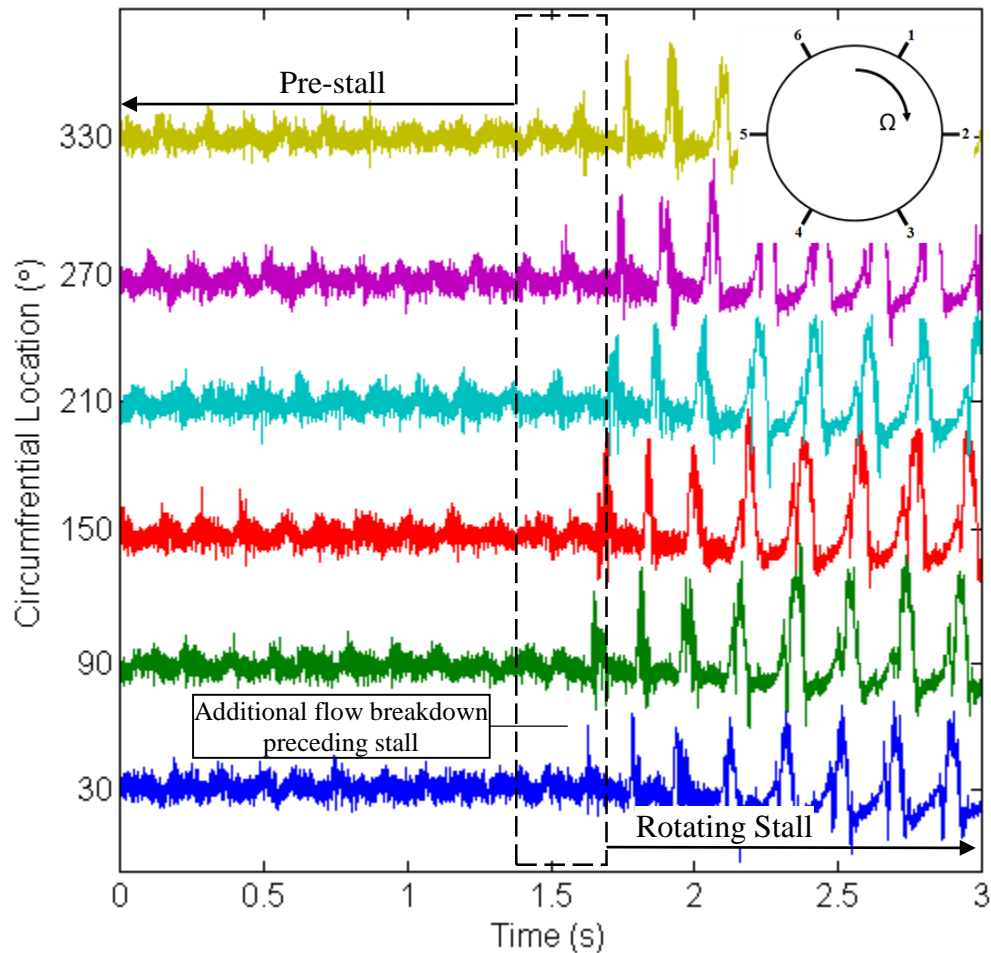
Figure 4-6: Filtered time variant pressure showing a stall inception event developing circumferentially.

The pre-stall disturbance and rotating stall cell also impact the entire span, as seen in Figure 4-7, which shows the hub transducer 40% rotor tip chord upstream compared to the one over the rotor leading edge with both transducers being at the 90° circumferential location for the same data set shown in Figure 4-6. The pre-stall disturbance was observed

to be in phase at both locations with the hub location showing the disturbance more clearly due to the blade passing response being lower upstream of the rotor blades.
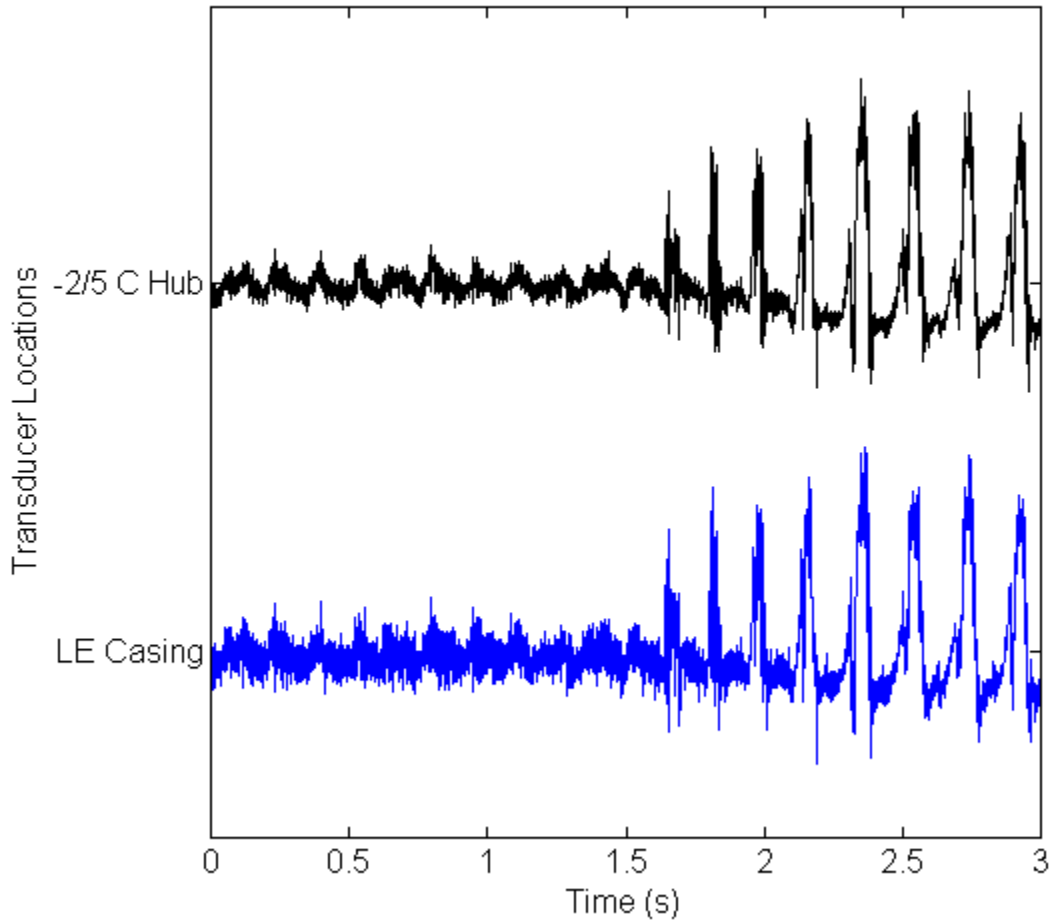
Figure 4-7: Filtered time variant pressure showing a stall inception event as seen across the span.

4.2.1.3 Cross-Spectrum Correlation

Cross-spectrum correlations were calculated using transducer pairs around the annulus in the rotor leading edge plane. The cross-spectrum correlations for the six transducer pairings at the compressor design point, flow coefficient of 0.54, are shown in Figure 4-8. The only significant frequency present is near 15 Hz, which corresponds to the rotor passing frequency and indicates during normal operation the compressor does not experience any disturbances of a frequency less than rotor rotation.
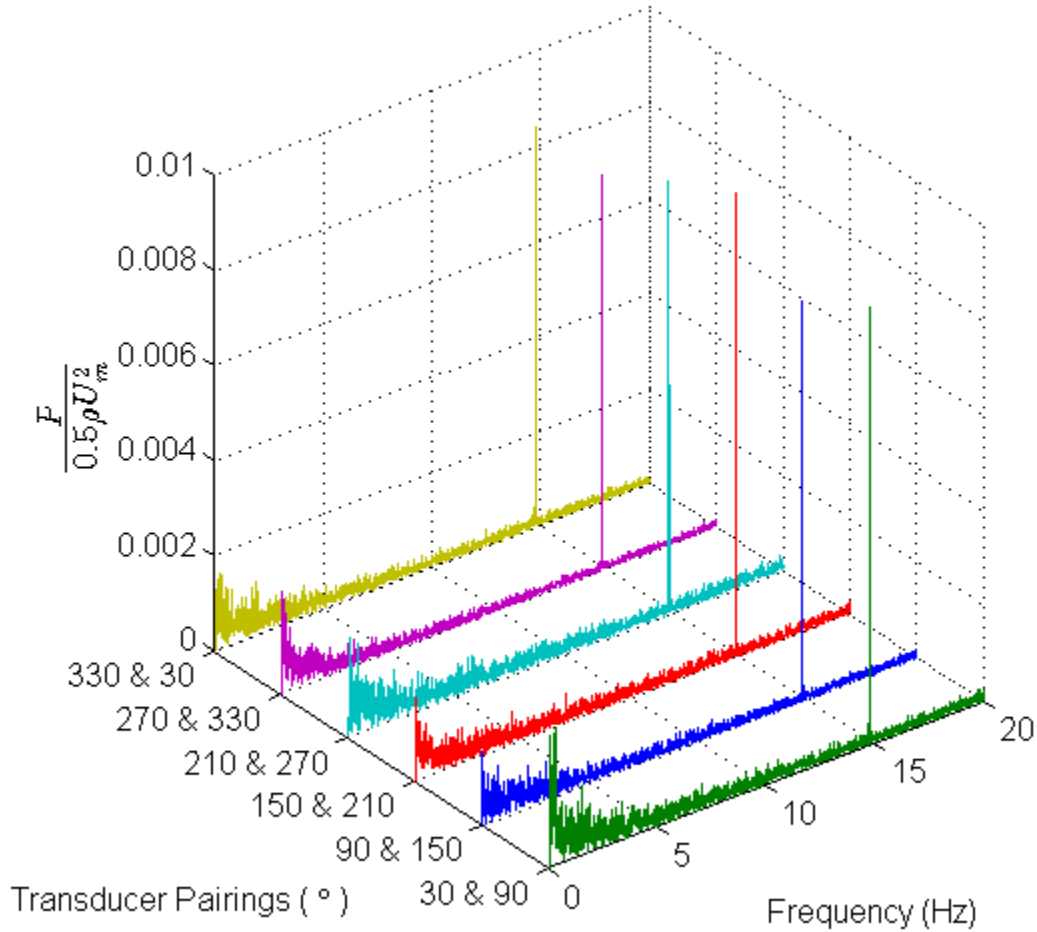
Figure 4-8: Cross-spectrum correlation of circumferential transducer pairings in the rotor leading edge plane at the design point.

The next set of cross-spectrum correlations are during the periodic disturbance at a flow coefficient below 0.4. In Figure 4-9, a frequency is present at close to 6.8 Hz. This frequency corresponds to the visible coherent low amplitude periodic disturbance. The overall amplitude of the pre-stall disturbance is on the same order as the one per revolution signature. After computing the phase angle and dividing by the transducer separation angle, the number of nodes was computed to be 2 for each of the transducer sets. This indicates that during the pre-stall disturbance the UKLSRC experiences a two node disturbance traveling at near 23% rotor rotational speed. These findings agree with, and further supplement, the hand calculations performed with the filtered time variant pressure.

36
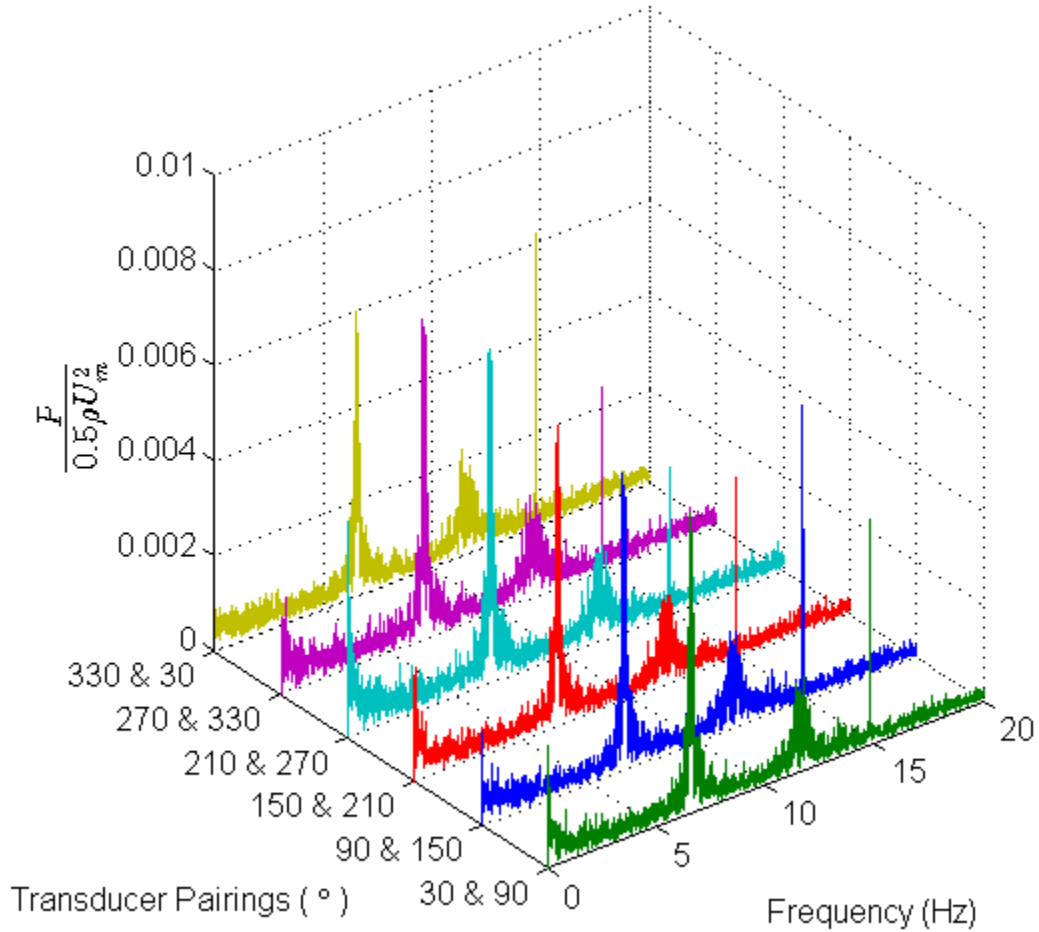
Figure 4-9: Cross-spectrum correlation of circumferential transducer pairings in the rotor leading edge plane.

The final set of circumferential cross-spectrum correlations occurs while the UKLSRC experiences fully developed rotating stall. A frequency near 5.2 Hz is prominently shown in Figure 4-10 while harmonics can be seen at the lower amplitudes. The magnitude of the rotating stall cell is more than an order of magnitude beyond the pre-stall disturbance and the rotor revolution signature. The number of cells at the fundamental stall frequency was calculated to be 1 for each of the transducer pairings. This shows that during fully developed rotating stall the UKLSRC experiences a single stall cell traveling at near 35% rotor rotational speed, which is consistent with the results from the filtered time variant pressure of Figure 4-4.
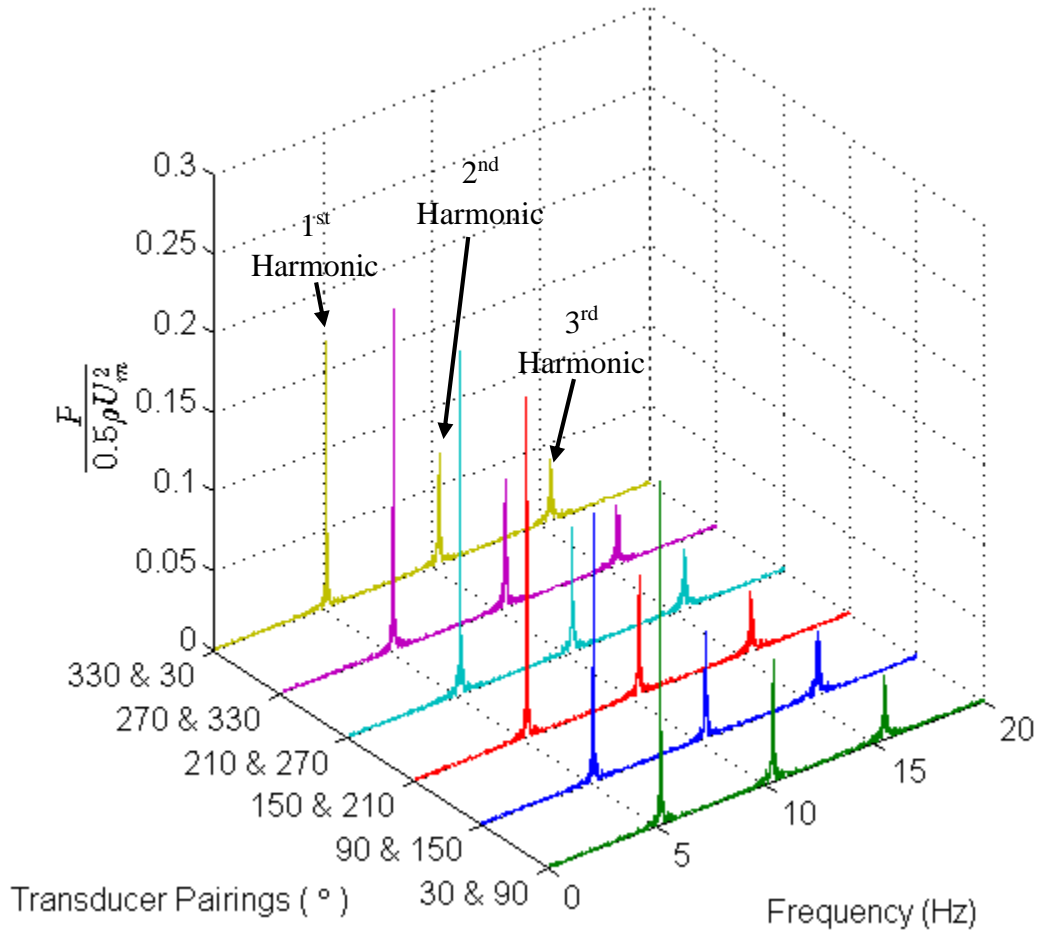
Figure 4-10: Cross-spectrum correlation of circumferential transducer pairings in the rotor leading edge plane during fully developed rotating stall.

4.2.1.4 Spatial Fourier Transform

With transducers equally spaced around the entire annulus in the rotor leading edge plane, a spatial Fourier transform was able to be conducted. For Figure 4-11, the compressor was operating below a flow coefficient of 0.4 and the pre-stall disturbance naturally transitioned into rotating stall. This is illustrated by a wavenumber of 2 being the largest amplitude before stall initiation near 41 seconds in which afterwards the wavenumber 1 becomes the predominant response. This can be related to the two node disturbance prior to single rotating stall cell becoming developed. This is also in agreement with the filtered time trace and cross-spectrum correlation results for the number of nodes during each operating condition.
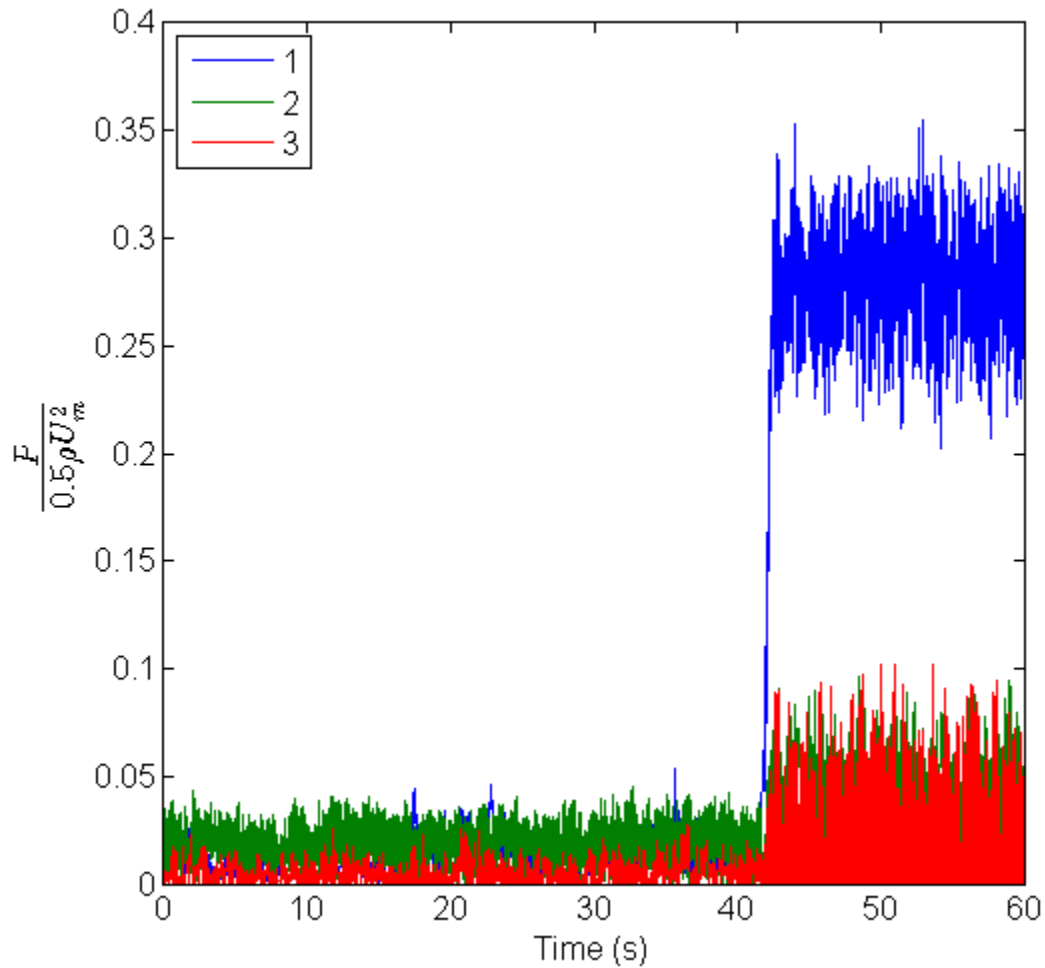
Figure 4-11: Spatial Fourier transform of a stall inception event showing the 2 node disturbance growing into a single rotating stall cell.

4.2.2 Axial Pressure Transducer Configuration

4.2.2.1 Flow Deviations

The trend present in the circumferential transducer configuration for the breakdown of flow periodicity as stall is approached is mimicked for the axial transducer configuration illustrated in Figure 4-12. While operating near the compressor design point with a flow coefficient of 0.54, there is not much spread in the amount of flow deviation along the rotor chord, but below a flow coefficient of 0.4 the breakdown at the rotor leading edge becomes dominate.
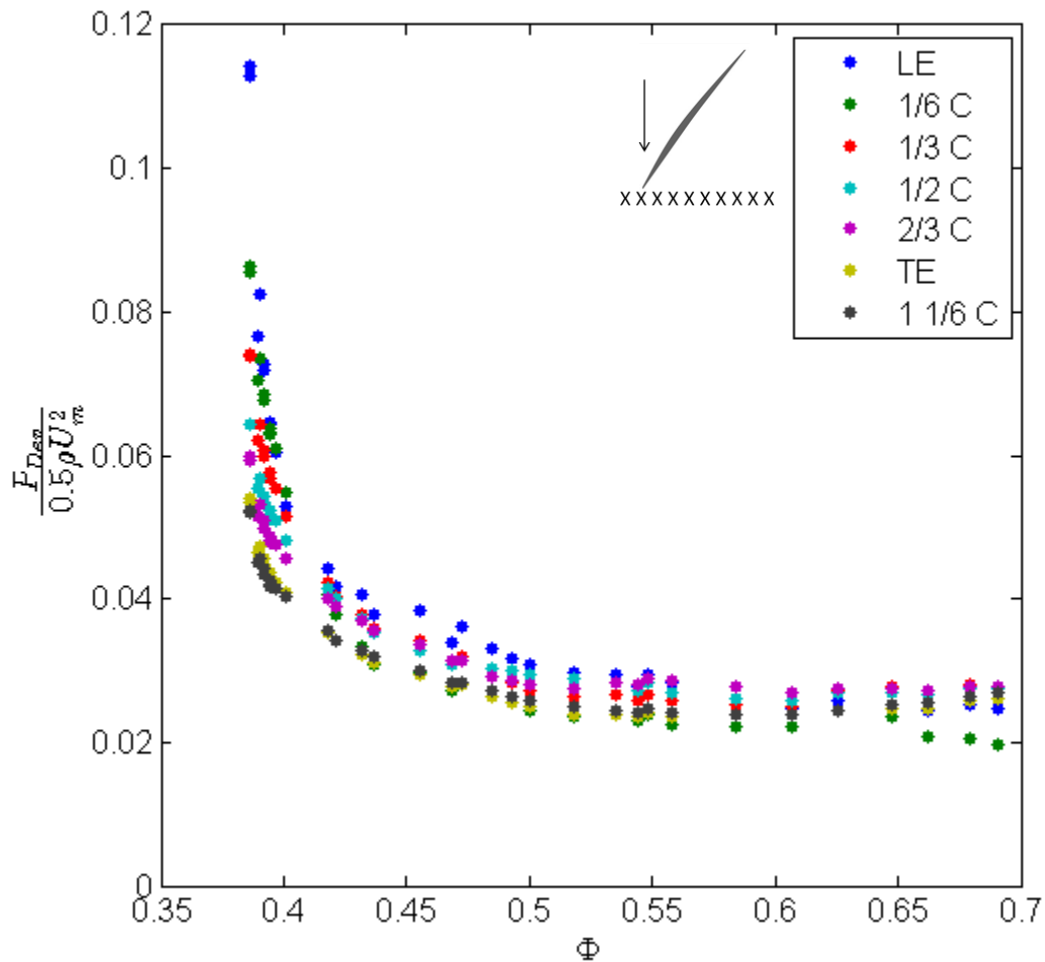
Figure 4-12: Blade periodicity deviations along the rotor chord showing the highest flow deviations occurring at the leading edge.

4.2.2.2 Time Dependent Pressures

The low-pass filtered time variant pressure measurements along the rotor chord length are presented in Figure 4-13 while the compressor is operating during rotating stall. It is evident that the stall cell is of enough size to impact the flow along the full length of the rotor tip chord. Visual inspection of Figure 4-13 shows 10 to 11 stall cell signatures over the two seconds for a frequency in the 5.25 Hz range, which is consistent for the circumferential cross-spectrum correlation frequency of near 5.2 Hz.
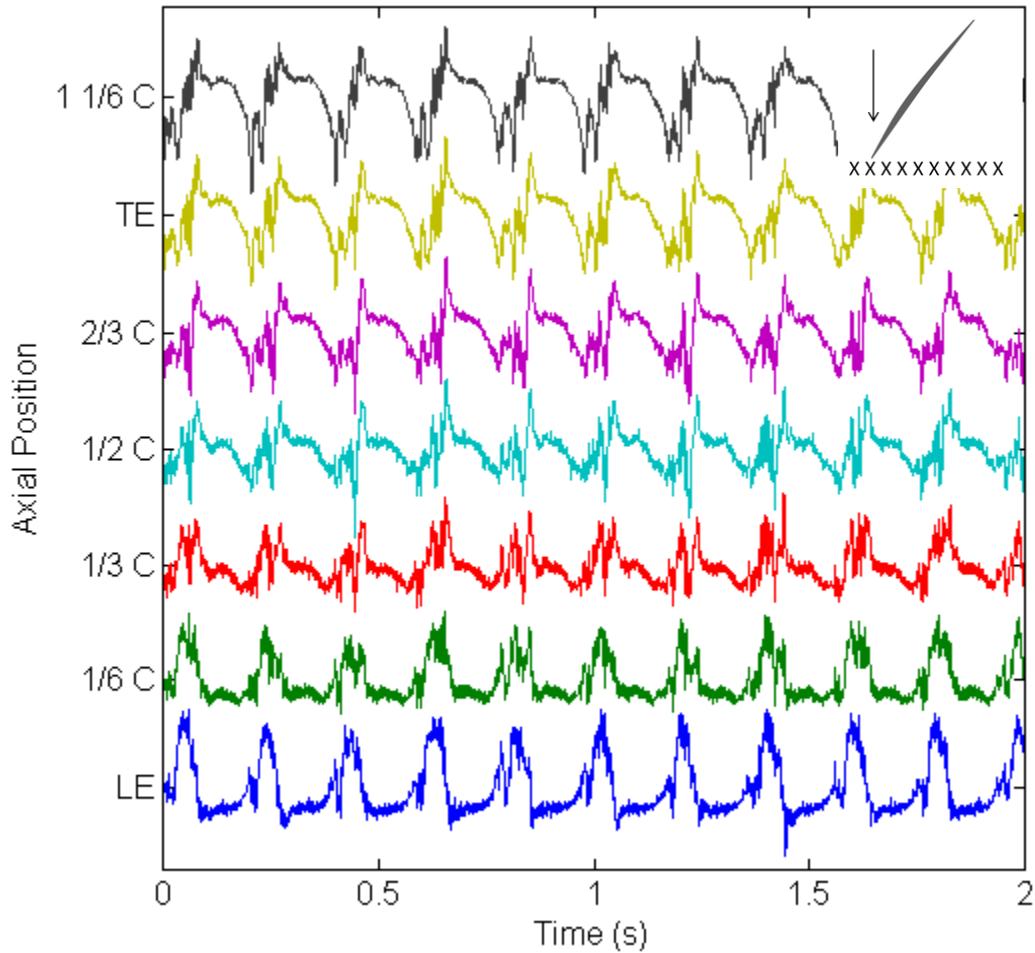
Figure 4-13: Filtered time trace along the axial chord.

Prior to stall and at a flow coefficient below 0.4 the pre-stall disturbance can be visually identified in the low-pass filtered time dependent pressure of Figure 4-14. This is an indication that the perturbed velocity field coming into the rotors is impacting the flow along the chord length and if a critical value is reached could lead to flow separating from the surface leading to stall.
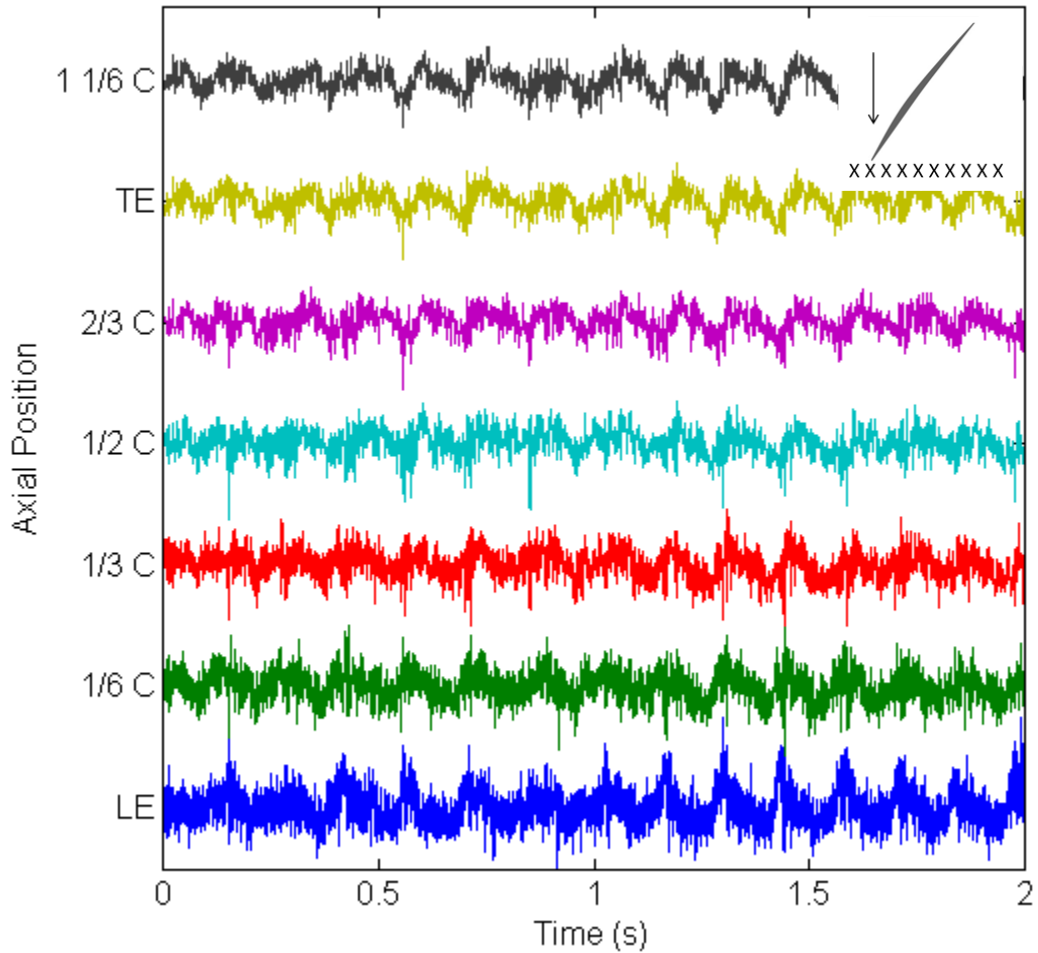
Figure 4-14: Filtered time dependent pressure showing the pre-stall disturbance along the axial chord.

A stall inception event is shown in the low-pass filtered time trace in Figure 4-15. At 0 seconds the compressor is operating with the modal disturbance and shortly after 0.5 seconds the rotating stall cell has been initiated elsewhere in the machine and it can be shown to grow in amplitude and size as it matures.
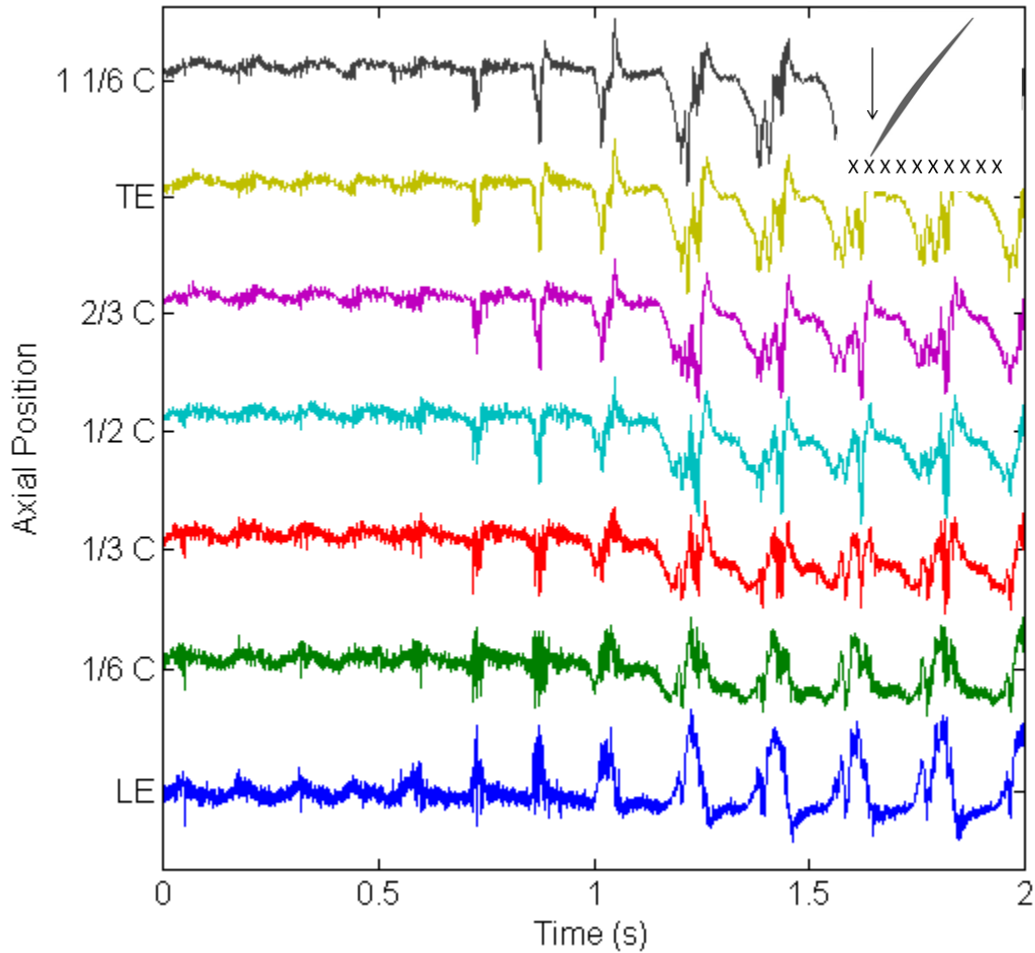
Figure 4-15: Stall inception event as seen along the rotor axial chord.

4.2.2.3 Fourier Transforms

Due to the transducers being spaced along the axial chord and not circumferentially spaced, cross-spectrum correlations were not able to be computed, but the Fourier transform of the pressure signal could still be analyzed. The Fourier transform of the pressure transducers while the compressor is operating at the design point, flow coefficient 0.54, is displayed in Figure 4-16. As with the cross-spectrum correlations of the circumferential transducer configuration, there are no frequencies below rotor passing frequency and the compressor is operating free of any disturbances.
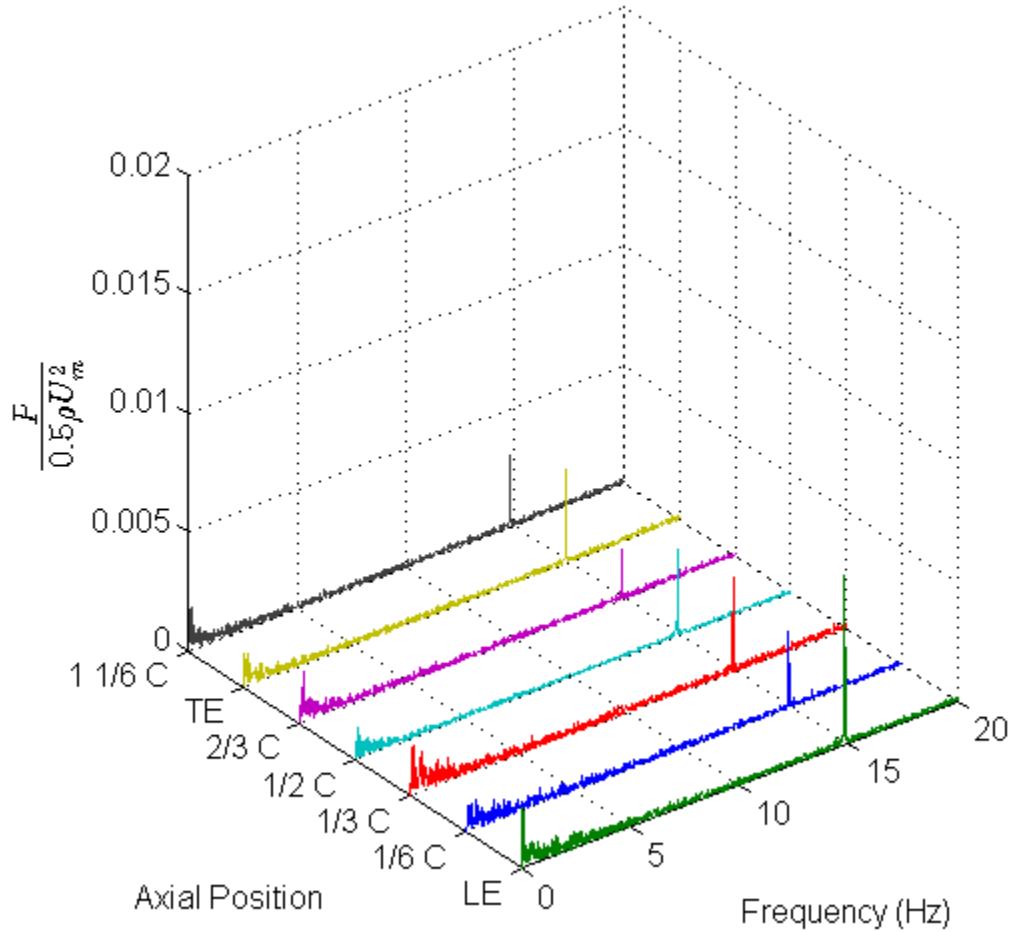
Figure 4-16: Fourier transform of pressure transducers located along the axial chord at the compressor design point.

The Fourier transform of the time variant pressure measurements presented in Figure 4-14 without the low-pass filtering is illustrated in Figure 4-17. The low amplitude periodic disturbance has a frequency near 6.8 Hz. This is in agreement with the prior cross-spectrum correlations performed with the circumferential pressure transducer arrangement. This confirms that the pre-stall disturbance impacts the rotor tip flow along the full chord length.
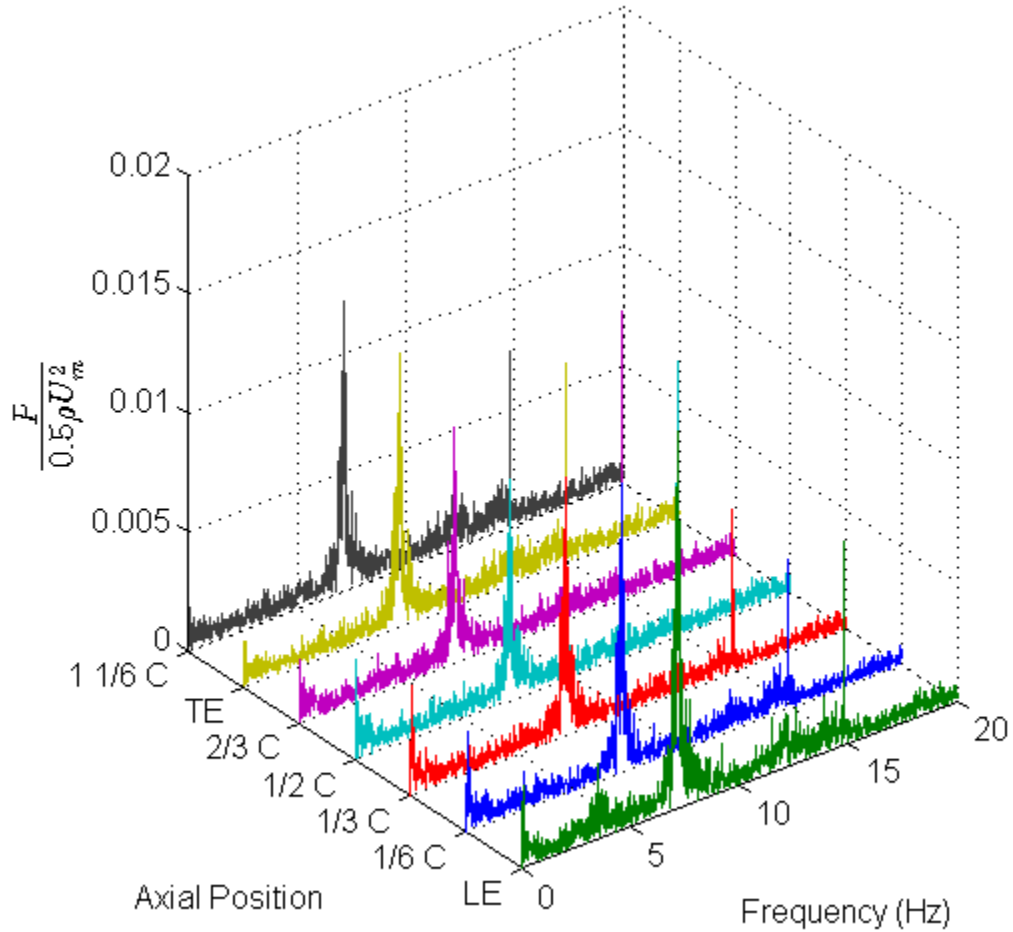
Figure 4-17: Fourier transform of pressure transducers located along the axial chord near the stall inception point.

For completeness, the Fourier transform during rotating stall is depicted in Figure 4-18 along the rotor tip chord. The near 5.2 Hz frequency and harmonics are predominant, as they were for the cross-spectrum correlations of the circumferential configuration during rotating stall. This also confirms that the stall cell heavily impacts the performance of the rotor tip flow along the chord length.
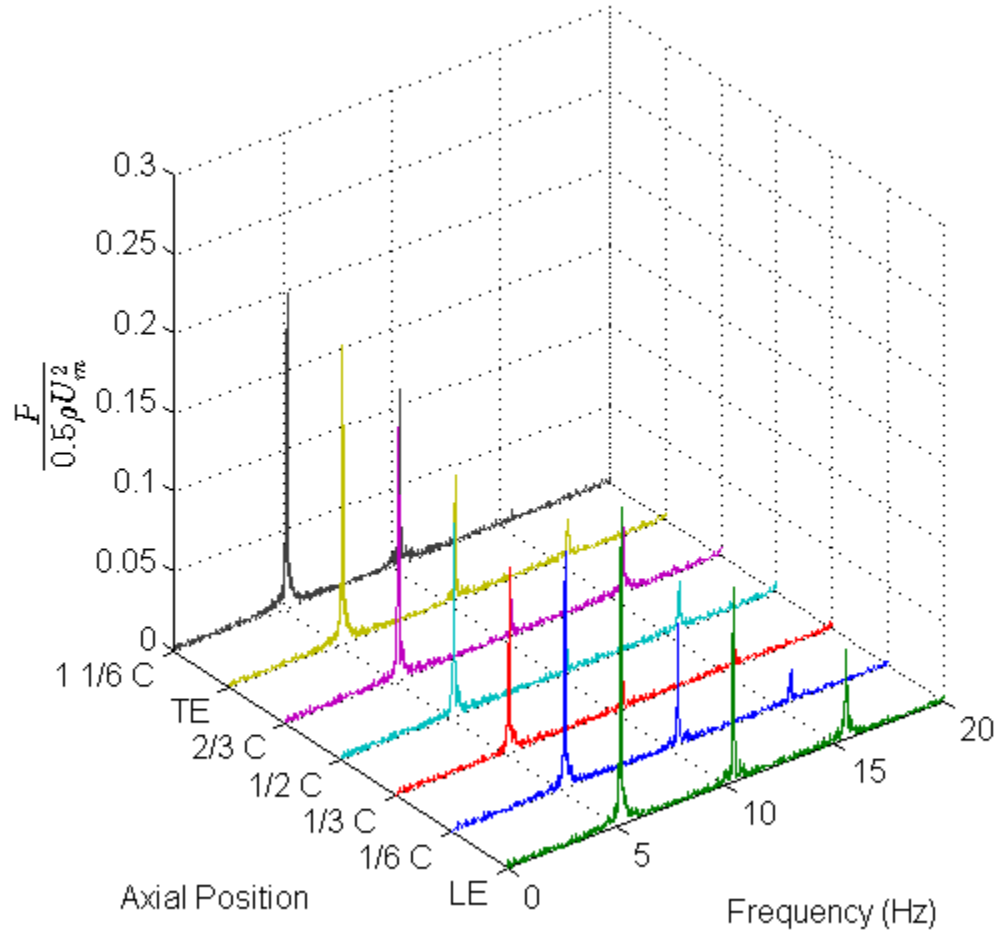
Figure 4-18: Fourier transform of pressure transducers located along the axial chord during fully developed rotating stall.

4.2.3 Rotor Pitch Pressure Transducer Configuration

4.2.3.1 Time Dependent Pressures

Having the pressure transducers located along one rotor blade pitch allows for a much finer spatial resolution, which is a benefit in the identification of spike stall initiation pre-cursors. The pre-stall disturbance illustrated in Figure 4-19 does not contain any classic stall pre-cursor events of high amplitude, short wavelength, pressure spikes. The low-pass filtered time dependent pressure continues to show the pre-stall disturbance that has appeared with the transducers in both prior configurations.
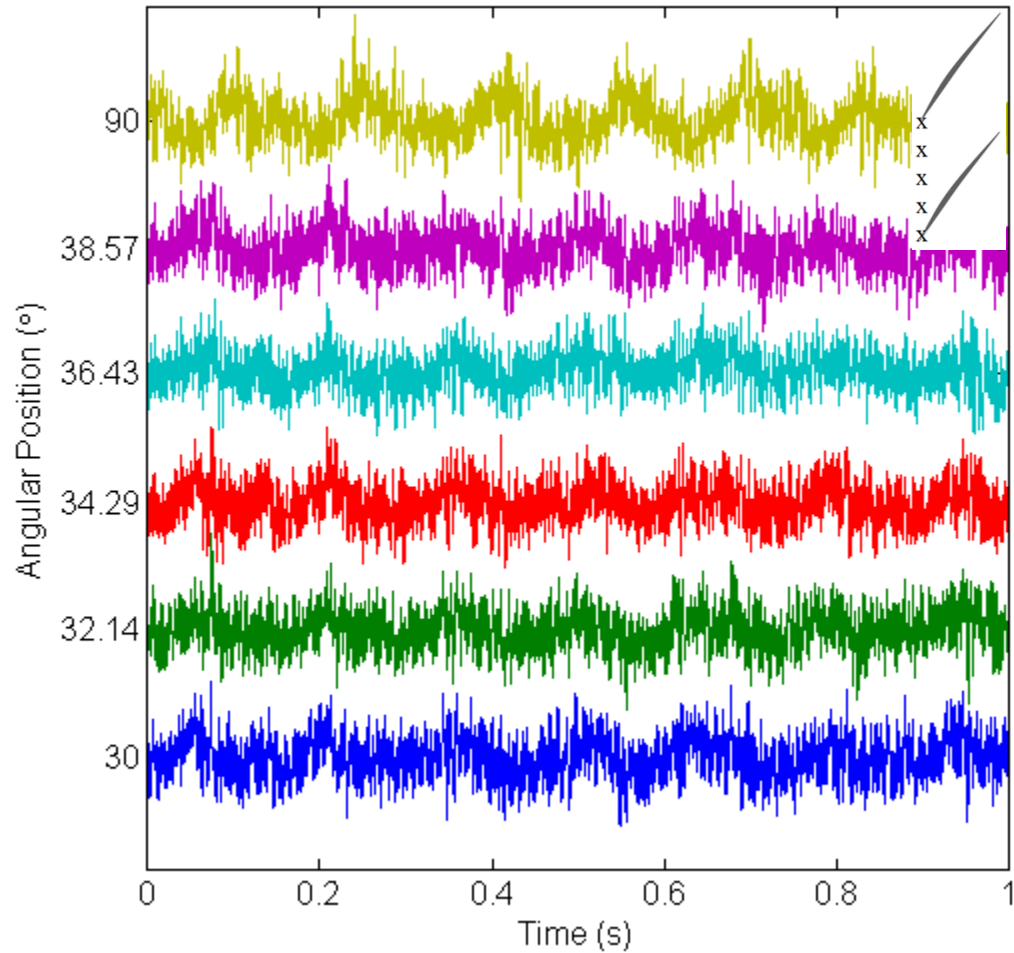
Figure 4-19: Filtered time dependent pressure showing the pre-stall disturbance along a rotor pitch with no indication of spike pre-cursors.

A stall initiation event is presented in Figure 4-20 illustrating the growth and development of the stall cell. At 0 seconds the compressor is operating with the pre-stall disturbance and shortly after 1.5 seconds the stall cell is growing that had been initiated elsewhere in the machine. The stall cell quickly matures into a full rotating stall. No evidence of high amplitude, short wavelength, events occur during stall inception were found.
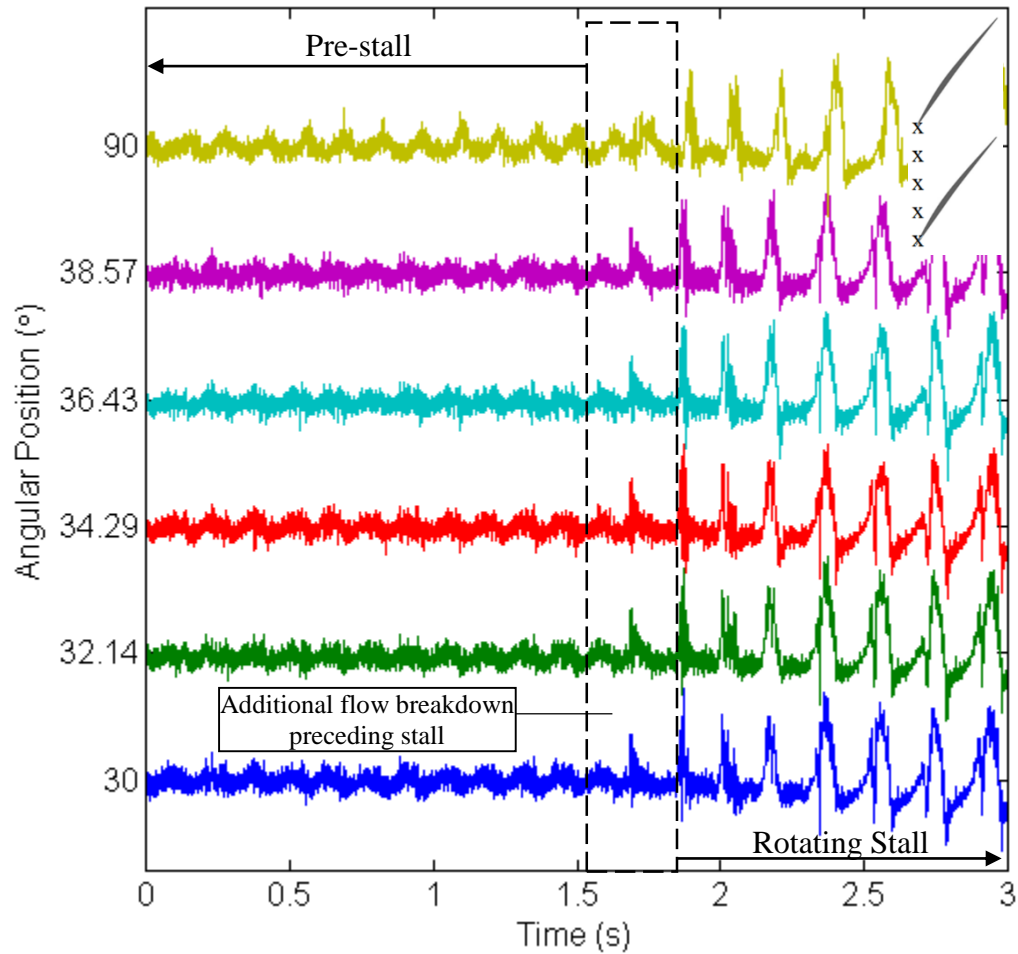
Figure 4-20: Filtered time dependent pressure showing the stall inception along a rotor pitch with no indication of spike pre-cursors.

4.2.3.2   Cross-Spectrum Correlation

By having the transducers closer spaced together, the angular separation decreases and the fidelity of the cross-spectrum correlation node calculation increases because of the higher number of nodes being able to be determined without aliasing. In the rotor pitch configuration transducer spacing of 2.14°, 8.57°, and 60° are available to use. These transducer sets provide a total number of non-aliased nodes to be calculated of 84, 21, and 3 respectively. The cross-spectrum correlation in Figure 4-21 occurs below a flow coefficient of 0.4 while the compressor is operating with the pre-stall disturbance. The near 6.8 Hz frequency is visible and considered to be a coherent structure. The number of nodes

calculated from the cross-power spectrum, for each transducer separation angle, still indicates that the pre-stall disturbance has 2 nodes.
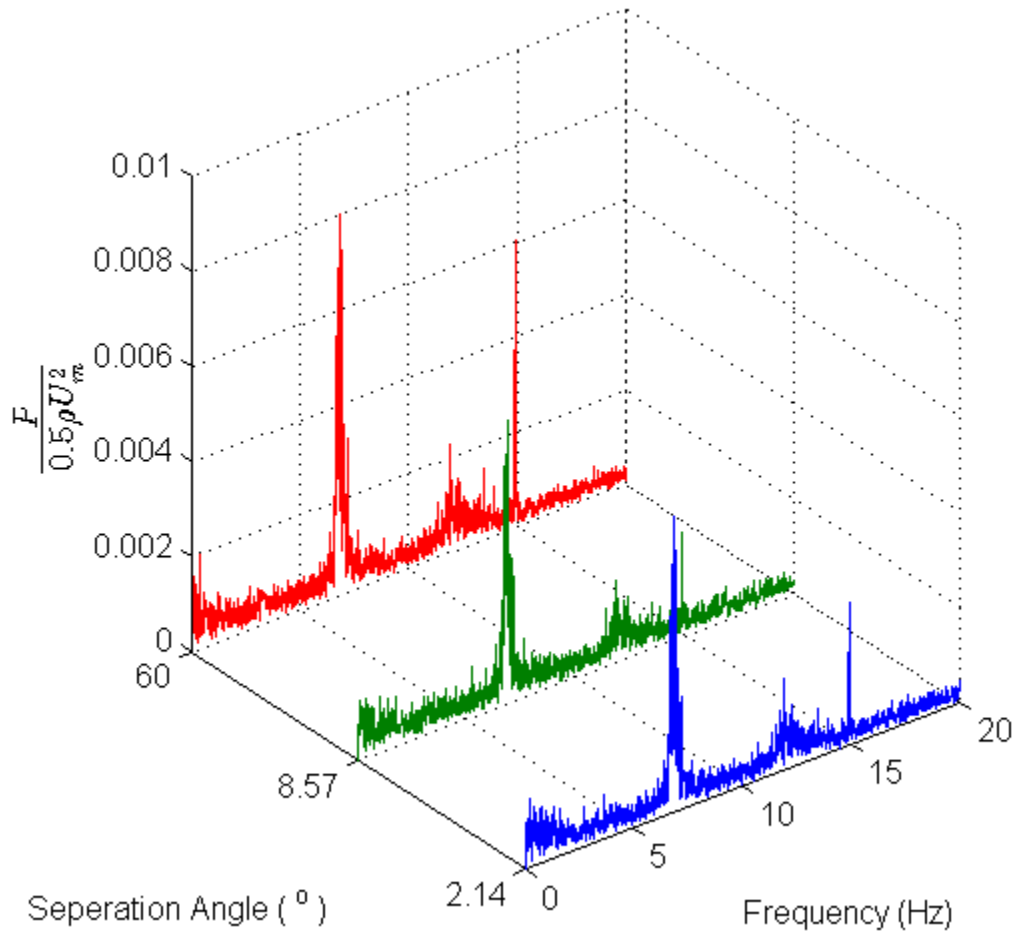
Figure 4-21: Cross-spectrum correlations along a rotor pitch during the pre-stall disturbance.

To verify the number of stall cells present during rotating stall, the cross-spectrum correlations were performed during rotating stall with the rotor pitch transducer configuration. The fundamental frequency response in Figure 4-22 is near 5.2 Hz and corresponds to the previously established stall cell frequency. Using the phase angle of the cross-power spectrum, the rotating stall has a single node.
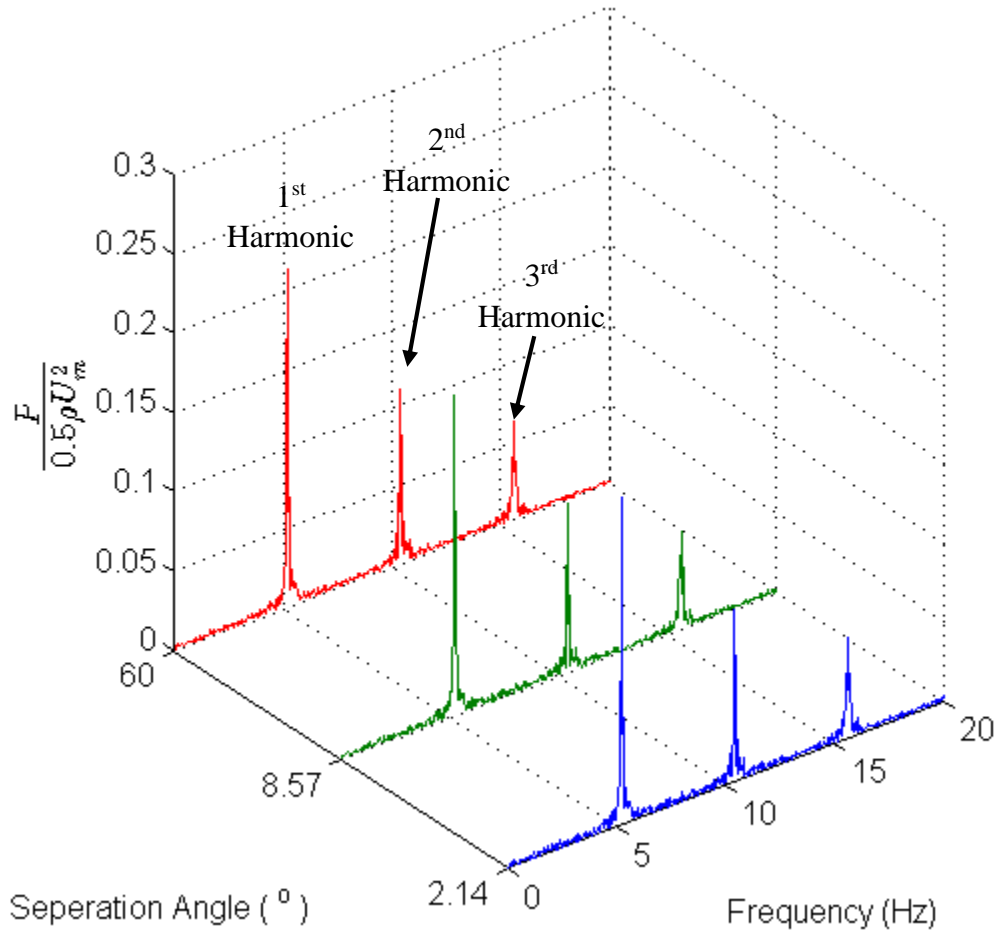
Figure 4-22: Cross-spectrum correlations along a rotor pitch during rotating stall.

4.3   Discussion

The data analysis consists of analyzing the breakdown of blade periodicity in terms of a standard deviation from the mean across a rotor revolution, cross-spectrum correlations between transducer pairings to determine coherent structures in the frequency spectrum, spatial Fourier transforms over time of the equally spaced circumferential transducers, and time traces of the pressure signals low-passed filtered at half of the blade passing frequency. These data analysis techniques were utilized to quantify the stall inception characteristics of the UKLSRC.

The breakdown of flow periodicity in the UKLSRC increases as the flow coefficient approaches the stall inception point. This is in good agreement with prior work by Young et al. (2011) who demonstrated a rise in the amount of flow irregularity as stall is approached in a single-stage low-speed compressor. The UKLSRC has a small mean tip clearance with a low level of eccentricity and the circumferential flow deviation measurements showing the same rate of growth support the findings of Young et al. (2011) for concentric compressors. The rotor leading edge transducer location showed the most sensitivity in regards to the breakdown of flow periodicity.

The UKLSRC behaves dimensionally similar at multiple rotational speeds. Steady state compressor characteristics show a near zero slope at the stall line while running at multiple rotational speeds and the pre-stall disturbance occurring below a flow coefficient of 0.4. The near zero slope is typical for a compressor that experiences a modal stall inception.

The cross-spectrum correlations were applied to the circumferential and rotor pitch transducer configurations, while standard Fourier transforms were applied to the axial chord configuration. The frequency spectrums for all transducer configurations were able to identify a pre-stall disturbance with a frequency near 6.8 Hz. By using the cross-spectrum correlations, the number of pre-stall nodes was found to be two. This corresponds to a two node pre-stall disturbance traveling near 23% rotor rotational speed. The pre-stall disturbance impacted the compressor span as seen from the frequency spectrum response of the pressure transducer located upstream of the rotors in the hub below a flow coefficient of 0.4. The frequency spectrums for all transducer configurations were able to detect the stall frequency of near 5.2 Hz. By using the cross-spectrum correlations the number of stall

51

cells was found to be one. This corresponds to a single stall cell traveling near 35% rotor rotational speed.

The low-pass filtered pressure traces allowed for easier visualization of the pre-stall disturbance. The low-pass filtering was also a requirement to perform the spatial Fourier transform for the circumferential transducer configuration. The spatial Fourier transform agreed with the number of nodes in the pre-stall disturbance and during rotating stall obtained by the cross-spectrum correlation. No indication of spike stall with large amplitude, short wavelength events were seen in the filtered pressure traces containing stall inception.

The transition from the pre-stall disturbance to a rotating stall occurs due to the change in incidence angle at the rotor leading edge. The pressure response can be correlated to a change in velocity and this velocity change could cause a blade or series of blades to have flow separation. If the amount of the flow separation is large enough to block the rotor passage, the rotor blade will stall and the stall will propagate through the compressor in the direction of rotation but at a slower speed.

All of the experimental results indicate the UKLSRC experiences a modal stall inception due to the following characteristics: 1) the compressor characteristics curve has a near zero positive slope at the stall inception point; 2) the coherent pre-stall disturbance exists for more than one hundred rotor revolutions prior to stall; 3) the coherent pre-stall disturbance is experienced across the span and through the entire annulus; 4) there is an up shift of rotational speed between the pre-stall disturbance and the rotating stall cell.

5 CONCLUSIONS

The instrumentation, data acquisition system, data analysis, and operating procedures were established to investigate the stall inception characteristics of the UKLSRC with a mean tip clearance 0.64% with respect to annulus height. The time variant instrumentation consisted of casing and hub mounted high frequency response pressure transducers that were used to quantify the static pressures at various transducer locations. The transducer configurations that were tested include being arranged equally spaced circumferentially around the annulus over the rotor leading edges, equally spaced within one rotor pitch in the leading edge plane, and equally spaced along the rotor axial chord length. The data acquisition system was created using the Data Acquisition Toolbox in MATLAB, which allows for continuous recording of the time variant data and TCP/IP connection to the Scanivavle pressure scanning unit. MATLAB was chosen due to the easy expandability in number of data acquisition channels.

The following conclusions can be drawn from this investigation:

1) Cross-spectrum correlations and spatial Fourier transforms are able to identify coherent structures and the number of nodes for modal stall inception. It is unclear if these methods would be applicable to spike stall inception.

2) For a limited number of pressure transducers, cross-spectrum correlations prove more effective than spatial Fourier transforms due to the spacing requirements of the spatial Fourier transform during modal stall inception.

3) Two pressure transducers in the same plane can be spaced close enough together to provide adequate anti-aliasing to determine the number of nodes.

4) The amount of breakdown of flow periodicity increases with a decrease in flow coefficient.

5) The UKLSRC experiences a modal stall inception.

Being able to better understand stall inception is important to the development and continued use of gas turbine engines. Greater understanding and control over stall can significantly reduce the cost in the design and development of turbomachines. Active stall control could help push gas turbine engines to new levels of performance as well as extend the gas turbine life cycle by reducing stall related fatigue.

A single experimental study has been presented that showcases the stall inception characteristics of the UKLSRC. The data analysis techniques present can be applied to any other low or high speed compressions systems to further study stall inception.

Data Acquisition MATLAB Code

Primary Data Acquisition

```
fclose('all'), clear all, close all, clc
global h8 s h4 fName lh fid1 a x P t h6 h5 V
Rate=100000;
a=1;
V=0;
s=daq.createSession('ni');

s.Rate=Rate;
x=linspace(0,1,Rate);
s.IsContinuous=1;
s.NotifyWhenDataAvailableExceeds=s.Rate;

s.addAnalogInputChannel('cDAQ1MOD1','ai0','Voltage');
s.addAnalogInputChannel('cDAQ1MOD1','ai1','Voltage');
s.addAnalogInputChannel('cDAQ1MOD1','ai2','Voltage');
s.addAnalogInputChannel('cDAQ1MOD1','ai3','Voltage');
s.addAnalogInputChannel('cDAQ1MOD3','ai0','Voltage');
s.addAnalogInputChannel('cDAQ1MOD3','ai1','Voltage');
s.addAnalogInputChannel('cDAQ1MOD3','ai2','Voltage');
s.addAnalogInputChannel('cDAQ1MOD3','ai3','Voltage');
s.addAnalogInputChannel('cDAQ1MOD4','ai0','Voltage');
s.addAnalogInputChannel('cDAQ1MOD4','ai1','Voltage');
s.addAnalogInputChannel('cDAQ1MOD4','ai2','Voltage');
s.addAnalogInputChannel('cDAQ1MOD4','ai3','Voltage');
s.addAnalogInputChannel('cDAQ1MOD5','ai0','Voltage');
s.addAnalogInputChannel('cDAQ1MOD5','ai1','Voltage');
s.addAnalogInputChannel('cDAQ1MOD5','ai2','Voltage');
s.addAnalogInputChannel('cDAQ1MOD5','ai3','Voltage');
s.addAnalogInputChannel('cDAQ1MOD8','ai2','Voltage');
s
t = tcpip('191.30.46.114', 23);
set(t, 'InputBufferSize', 30000);
fopen(t);
fprintf(t,'set chan1 0');
fscanf(t)
fprintf(t,'set chan1 1-1..2-16');
fscanf(t)
fprintf(t,'set avg 30');
fscanf(t)
fprintf(t,'set fps1 1');
fscanf(t)
fprintf(t,'set unitscan pa');
fscanf(t)

h=figure;
lh2 = s.addlistener('DataAvailable', @plotData);

h8=uicontrol('Style','popupmenu','String',[1:length(s.Channels)],'uni
ts','normalized','Position', [0.01 0.31 0.08 0.05]);
```

```matlab
h0=uicontrol('Style','pushbutton','String','Run','units','normalized'
,'Position', [0.01 0.949 0.08 0.05], 'Callback',
's.startBackground');
h4=uicontrol('Style','edit','String','TypeDesiredFileNameHere','units
','normalized','Position', [0.4 0.01 0.20 0.049]);
h1=uicontrol('Style','pushbutton','String','End','units','normalized'
,'Position', [0.92 0.01 0.08 0.05], 'Callback', 's.stop');
h2=uicontrol('Style','pushbutton','String','Save','units','normalized
','Position', [0.1 0.01 0.08 0.05], 'Callback', 'SaveData');
h3=uicontrol('Style','pushbutton','String','Reset','units','normalize
d','Position', [0.01 0.01 0.08 0.05], 'Callback', 'ResetData');
h5=uicontrol('Style','text','String',sprintf('%2.3f',V),'units','norm
alized','Position', [0.92 0.949 0.08 0.05]);
h6=uicontrol('Style','text','String',sprintf('%1.0f',a),'units','norm
alized','Position', [0.92 0.91 0.08 0.05]);
```

Secondary Data Acquisition For Scanivalve

```matlab
global P t
disp('Scani started')
for I=1:30
    fprintf(t,'scan');
    pause(1.8)
    q=1;
    while q<=33
        q;
        t.BytesAvailable;
        DataReceived = fscanf(t) ;
        c = textscan(DataReceived, '%s%s%s%d%f64');
        if (~isnan(c{5}));
            P(I,q)=c{5};
        end
        q=q+1;
    end
end
save(sprintf('SV%s.mat',fName),'P')
P=[];
disp('Scani done')
```

Required Functions

```matlab
function ResetData
global h4 fName fid1 lh s a
fName=get(h4,'String');
fclose('all');
fid1 = fopen(sprintf('%s.bin',fName),'w');
lh = s.addlistener('DataAvailable',@(src, event)logData(src, event,
fid1));
disp('Data Recording Started')
a=1;
Scani
end
```

```matlab
function SaveData
global fName fid1 lh h4 s a
s.stop;
delete(lh);
fclose(fid1);
s.startBackground
a=1;
disp('Data Saved')
end
```

```matlab
function plotData(src,event)
global  h1 h2 h3 h8 h5 fid1 lh h4 fName s a h6 V x h
ps=get(h8,'Value');
plot(x,event.Data(:,ps),'.');
V=(mean(event.Data(:,1))-0.7675)/0.038164;
set(h5,'String',V)
set(h6,'String',a)
a=a+1;
end
```

Data Processing Code

```
  clear, clc
CPT=cputime;
list= dir('File_Name');
listSV=dir('SV_File_Name');
Z=1;

for Q=1:length(list)
    tic
    fName=list(Q).name
    fid2 = fopen(fName,'r');
    [data]= fread(fid2,[14,inf],'double');
    fclose(fid2);
    data=data';
    toc
    load('offsets.mat')              %Contains Kulite constants
%% Data Trailing Zeros Check
    d1=data(:,1);
    ld=length(d1);
    d1=d1(d1~=0);
    if length(d1)~=ld
        l=floor(length(d1)/100000);
        data=data([1:l*100000],:);
        disp('ERROR: Trailing Zeros')
    end
    clear d1 ld l
%% Constants
    RPM=881;                         %Rotor Revolutions Per Minute
    Patm=99898;                      %Atmospheric Pressure (Pa)
    Ro=287.058;
    Ainlet=0.420283451462628;        %Compressor Inlet Area (m^2)
    Length=2;                        %Lever arm length (m)
    Um=0.54864*pi*2*(RPM/60);        %Mean Blade Speed (m/2)

%% Voltage to Pressure
    t=data(:,1);                     %Time
    K1=(data(:,10)-offs(10))*c1;
    K2=(data(:,13)-offs(13))*c2;
    K3=(data(:,7)-offs(7))*c3;
    K4=(data(:,9)-offs(9))*c4;
    K5=(data(:,11)-offs(11))*c5;
    K6=(data(:,12)-offs(12))*c6;
    KU=(data(:,8)-offs(8))*c7;
    KD=(data(:,6)-offs(6))*c8;
%% Optical Sensor Triggers
    c=1;
    z=find((5)<=data(:,3));          %Finds all triggered voltages
    for n=1:length(z)-1              %Loop to find voltage rise leading
edge
        a(n)=z(n+1)-z(n);
        if a(n)>3000 & 8000>a(n)
            d1(c)=z(n+1);
            c=c+1;
        elseif a(n)>=8000            %Checks for trigger failures
            d1(c+1)=z(n+1);
```

58

```matlab
            d1(c)=round((d1(c-1)+d1(c+1))/2);
            c=c+2;
            disp 'Optical Sensor Failure'
            z(n)
        end
    end
    b=diff(d1);                          %Timing between Revolutions
    if Z==1
        ZZ=ceil(mean(b)/42)*42;
    end
    zz=linspace(0,1,ZZ);
%% Revolution Based Splitting
    for o=1:length(d1)-1
        k1=K1(d1(o):d1(o+1));
        xx=linspace(0,1,length(k1));
        kk1=interp1(xx,k1,zz);
        KL1(o,:)=kk1;
    end
    for o=1:length(d1)-1
        k2=K2(d1(o):d1(o+1));
        xx=linspace(0,1,length(k2));
        kk2=interp1(xx,k2,zz);
        KL2(o,:)=kk2;
    end
    for o=1:length(d1)-1
        k3=K3(d1(o):d1(o+1));
        xx=linspace(0,1,length(k3));
        kk3=interp1(xx,k3,zz);
        KL3(o,:)=kk3;
    end
    for o=1:length(d1)-1
        k4=K4(d1(o):d1(o+1));
        xx=linspace(0,1,length(k4));
        kk4=interp1(xx,k4,zz);
        KL4(o,:)=kk4;
    end
    for o=1:length(d1)-1
        k5=K5(d1(o):d1(o+1));
        xx=linspace(0,1,length(k5));
        kk5=interp1(xx,k5,zz);
        KL5(o,:)=kk5;
    end
    for o=1:length(d1)-1
        k6=K6(d1(o):d1(o+1));
        xx=linspace(0,1,length(k6));
        kk6=interp1(xx,k6,zz);
        KL6(o,:)=kk6;
    end
    for o=1:length(d1)-1
        k7=KD(d1(o):d1(o+1));
        xx=linspace(0,1,length(k7));
        kk7=interp1(xx,k7,zz);
        KDL(o,:)=kk7;
    end
    for o=1:length(d1)-1
        k8=KU(d1(o):d1(o+1));
```

```matlab
        xx=linspace(0,1,length(k8));
        kk8=interp1(xx,k8,zz);
        KUL(o,:)=kk8;
    end
%% Mean Pressure Profiles
    MP1=mean(KL1);
    MP2=mean(KL2);
    MP3=mean(KL3);
    MP4=mean(KL4);
    MP5=mean(KL5);
    MP6=mean(KL6);
    MPU=mean(KUL);
    MPD=mean(KDL);
    MCP(:,:,Q)=[MP1;MP2;MP3;MP4;MP5;MP6;MPU;MPD];
%% Standard Deviations
    SK1=std(KL1);
    SK2=std(KL2);
    SK3=std(KL3);
    SK4=std(KL4);
    SK5=std(KL5);
    SK6=std(KL6);
    SKU=std(KUL);
    SKD=std(KDL);
    Dev(:,Q)=[mean(SK1) mean(SK2) mean(SK3) mean(SK4) mean(SK5)
mean(SK6) mean(SKU) mean(SKD)];
%% Half BPF Filters
    tic
    Fc=310;
    fNorm = Fc / (100000/2);
    [b,a] = butter(4, fNorm, 'low');
    f1 = filter(b, a, K1);
    f2 = filter(b, a, K2);
    f3 = filter(b, a, K3);
    f4 = filter(b, a, K4);
    f5 = filter(b, a, K5);
    f6 = filter(b, a, K6);
    fd = filter(b, a, KD);
    fu = filter(b, a, KU);
    clear fNorm b a
    toc
%% Fourier Transforms
    L=length(K1);
    Fs=100000;
    y1=2*abs(fft(K1-mean(K1))/L);
    y2=2*abs(fft(K2-mean(K2))/L);
    y3=2*abs(fft(K3-mean(K3))/L);
    y4=2*abs(fft(K4-mean(K4))/L);
    y5=2*abs(fft(K5-mean(K5))/L);
    y6=2*abs(fft(K6-mean(K6))/L);
    yu=2*abs(fft(KU-mean(KU))/L);
    yd=2*abs(fft(KD-mean(KD))/L);
    fre=Fs/2*linspace(0,1,L/2+1);
%% Steady State Scanivalve Processing
    Vo=data(:,4);
    Ve=data(:,5);
    Rr=993;
```

```matlab
    R=Vo.*(Rr./(Ve-Vo));
    A=1.468*10^-3;
    B=2.383*10^-4;
    C=1.007*10^-7;
    T=(A+B*log(R)+C*(log(R).^3)).^-1;
    Temp(Q)=mean(abs(T));
    ro(Q)=Patm/(Ro*Temp(Q));
    fName=listSV(Q).name;
    load(fName);
    meandata=mean(P);
    meanSV(Q,:)=meandata;
    SS(Q,1)=mean(meandata([17:20]));    %Casing Inlet
    SS(Q,2)=mean(meandata(21:24));      %Hub Inlet
    SS(Q,3)=mean(meandata([21:23]));    %Casing Exit
    SS(Q,4)=SS(Q,3)-SS(Q,1);           %Pressure Rise
    SS(Q,5)=sqrt((-2*SS(Q,1))/ro(Q));  %Inlet Velocity Casing
    SS(Q,6)=(ro(Q)*(((48)/2)^2-
((48*.8)/2)^2))*pi)*0.00064516*SS(Q,5); %Mass Flow
    SS(Q,7)=((SS(Q,6)*SS(Q,4))/ro(Q))*0.00134102209;   %Hp Aero
    SS(Q,8)=SS(Q,5)/Um;                %Flow Coef Casing
    SS(Q,9)=SS(Q,3)/(.5*ro(Q)*Um^2);   %Pressure Coef
%% Cross Spectrum Correlations
    tic
    a1=fft(K1)/L;
    a2=fft(K2)/L;
    a3=fft(K3)/L;
    a4=fft(K4)/L;
    a5=fft(K5)/L;
    a6=fft(K6)/L;
    toc
    tic
    c12=a1.*conj(a2);
    c23=a2.*conj(a3);
    c34=a3.*conj(a4);
    c45=a4.*conj(a5);
    c56=a5.*conj(a6);
    c61=a6.*conj(a1);
    toc
    tic
    A12=2*sqrt(abs(c12));
    A23=2*sqrt(abs(c23));
    A34=2*sqrt(abs(c34));
    A45=2*sqrt(abs(c45));
    A56=2*sqrt(abs(c56));
    A61=2*sqrt(abs(c61));
    toc
    tic
    P12=rad2deg(angle(c12));
    P23=rad2deg(angle(c23));
    P34=rad2deg(angle(c34));
    P45=rad2deg(angle(c45));
    P56=rad2deg(angle(c56));
    P61=rad2deg(angle(c61));
    toc
%% Spatial FT
    tic
```

```matlab
    Fc=9;
    fNorm = Fc / (100000/2);
    [b,a] = butter(4, fNorm, 'low');
    g1 = filter(b, a, K1-mean(K1));
    g2 = filter(b, a, K2-mean(K2));
    g3 = filter(b, a, K3-mean(K3));
    g4 = filter(b, a, K4-mean(K4));
    g5 = filter(b, a, K5-mean(K5));
    g6 = filter(b, a, K6-mean(K6));
    gd = filter(b, a, KD-mean(KD));
    gu = filter(b, a, KU-mean(KU));
    clear fNorm b a
    toc
    sft0=zeros(1,length(K1));
    sft1=sft0;sft2=sft1;sft3=sft2;
    tic
    for i=1:length(K1)
        temp=[g1(i) g2(i) g3(i) g4(i) g5(i) g6(i)];
        fftem=fft(temp)/6;
        fftemp=2*abs(fftem);
        aft0(i)=rad2deg(angle(fftem(1)));
        aft1(i)=rad2deg(angle(fftem(2)));
        aft2(i)=rad2deg(angle(fftem(3)));
        aft3(i)=rad2deg(angle(fftem(4)));
        sft0(i)=fftemp(1);
        sft1(i)=fftemp(2);
        sft2(i)=fftemp(3);
        sft3(i)=fftemp(4);
    end
    toc
%%
    Z=Z+1;
    clearvars -except Q Dev Ev list CPT Lc MCP diff O OO CR1 CR2 CR3
CR4 CR5 CR6 CRM Z SS ZZ listSV ro Temp meanSV Freq Amp RMSK1 RMSK2
RMSK3 RMSK4 RMSK5 RMSK6 RMSKU RMSKD
end
```

REFERENCES

Beckwith, T., Marangoni. R., and Lienhard, J., *Mechanical Measurements*. Upper Saddle River, NJ: Pearson/Prentice Hall, 2007.

Camp, T. and Day, I., "A Study of Spike and Modal Stall Phenomena in a Low-Speed Axial Compressor," *Journal of Turbomachinery*, Vol. 120, July, 1998, pp. 393-401.

Day, I.J., "Stall Inception in Axial Flow Compressors," *Journal of Turbomachinery*, Vol. 115, Jan, 1993, pp. 1-9.

Fleeter, S., Bennett, W. A., and Jay, R. L., "The Time-Variant Aerodynamic Response of a Stator Row Including the Effects of Airfoil Camber," *Journal of Engineering for Power*, Vol. 102, pp. 334-343.

Greitzer, M., "The Stability of Pumping Systems – The 1980 Freeman Scholar Lecture," Journal of Fluids Engineering, Vol. 103, 1981, pp. 193-242.

Kulite, "Miniature Ruggedized Pressure Transducer XT-190 (M) Series," Web, April, 2014.

McDougall, N., Cumpsty, N., and Hynes, T., "Stall Inception in Axial Compressors," *Journal of Turbomachinery*, Vol. 112, Jan, 1990, pp. 116-125.

Moore, F. and Greitzer, E., "A Theory of Post-Stall Transients in Axial Compression Systems: Part I-Development of Equations," *Journal of Engineering for Gas Turbines and Power*, Vol. 108, Jan, 1986, pp. 68-76.

Stenning, A., "Rotating Stall and Surge," *Journal of Fluids Engineering*, Vol. 102, March, 1980, pp. 14-20.

Young, A., Day, I., and Pullan, G., "Stall Warning By Blade Pressure Signature Analysis," *Proceedings of ASME Turbo Expo 2001*, GT2011-45850.

VITA

Name: Bradley David Butler

Place of Birth: Paducah, Kentucky

Education:

- Bachelor of Science in Mechanical Engineering, University of Kentucky, 2012

Professional positions held:

- Teaching Assistant, University of Kentucky, Spring 2014

- Graduate Research Assistant, University of Kentucky, 2012-2014

- Undergraduate Research Assistant, University of Kentucky, 2010-2012

Scholastic honors:

- Graduated University of Kentucky Magna Cum Laude

- NASA Kentucky EPSCoR Space Grant recipient

Professional Publications:

Butler, B. and Capece, V., 2014, "Unsteady Pressure Measurements of a Low-Speed Single-Stage Axial-Flow Compressor Near Stall," *Presentations 39th Dayton-Cincinnati Aerospace Science Symposium.*

Whipple, W., Butler, B., Sterrie, C., and Seay, J., 2013, "A Sustainable Low Cost Process For The Production Of Biodiesel Suitable For Underdeveloped Regions," *Journal of Green Building*, Vol. 8, No3. pp. 140-155.

Butler, B. and Capece, V., 2013, "Casing Dynamic Pressure Measurements of an Axial Flow Compressor Near Stall," *KY EPSCoR Annual Conference*.

Butler, B. and Capece, V., 2013, "Time-dependent Shroud Pressure Measurements of a Single-stage Compressor Near Rotating Stall Inception," *Presentations 38th Dayton-Cincinnati Aerospace Science Symposium.*

Seay, J., Zama, I., and Butler, B., 2012, "International Partnership Helping to Bring Appropriate Biofuel Technology to Rural Cameroon," *International Journal of Service Learning in Engineering,* Vol. 7, No. 2.

Butler, B. and Capece, V., 2012, "Performance Measurements of a Low-Speed Single-Stage Axial-Flow Compressor," *AIAA Paper No. AIAA*-2012-3726.

Butler, B. and Capece, V., 2012, "Performance Measurements of the University of Kentucky Low-Speed Axial-Flow Compressor," *Presentations 37th Dayton-Cincinnati Aerospace Science Symposium.*

Butler, B., Sterrie, C., and Whipple, W., 2012, "Cameroon Biodiesel Project," *Papers MESCON, University of Evansville.*

Butler, B., 2012, "Optimization of a Rotor Blade Vibration Control System," *Presentations MESCON, University of Evansville.*